LUMPED ELEMENT MODELING OF CIRCULAR CMUT IN COLLAPSED MODE

A DISSERTATION SUBMITTED TO
THE DEPARTMENT OF ELECTRICAL AND ELECTRONICS ENGINEERING
AND THE GRADUATE SCHOOL OF ENGINEERING AND SCIENCE
OF BILKENT UNIVERSITY
IN PARTIAL FULFILLMENT OF THE REQUIREMENTS
FOR THE DEGREE OF
DOCTOR OF PHILOSOPHY

By
Elif Aydoğdu
January, 2014

In reference to IEEE copyrighted material which is used with permission in this thesis, the IEEE does not endorse any of Bilkent University's products or services. Internal or personal use of this material is permitted. If interested in reprinting/republishing IEEE copyrighted material for advertising or promotional purposes or for creating new collective works for resale or redistribution, please go to http://www.ieee.org/publications_standards/publications/rights/rights_link.html to learn how to obtain a License from RightsLink.

I certify that I have read this thesis and that in my opinion it is fully adequate, in scope and in quality, as a dissertation for the degree of Doctor of Philosophy.

Prof. Dr. Abdullah Atalar(Advisor)

I certify that I have read this thesis and that in my opinion it is fully adequate, in scope and in quality, as a dissertation for the degree of Doctor of Philosophy.

Prof. Dr. Hayrettin Köymen(Co-Advisor)

I certify that I have read this thesis and that in my opinion it is fully adequate, in scope and in quality, as a dissertation for the degree of Doctor of Philosophy.

Prof. Dr. Ergin Atalar

I certify that I have read this thesis and that in my opinion it is fully adequate, in scope and in quality, as a dissertation for the degree of Doctor of Philosophy.

Prof. Dr. Atilla Aydınlı

I certify that I have read this thesis and that in my opinion it is fully adequate, in scope and in quality, as a dissertation for the degree of Doctor of Philosophy.

Assoc. Prof. Dr. Arif Sanlı Ergün

I certify that I have read this thesis and that in my opinion it is fully adequate, in scope and in quality, as a dissertation for the degree of Doctor of Philosophy.

Asst. Prof. Dr. Coşkun Kocabaş

Approved for the Graduate School of Engineering and Science:

Prof. Dr. Levent Onural
Director of the Graduate School

Copyright Information

©2014 IEEE. Reprinted, with permission, from E. Aydogdu, A. Ozgurluk, A. Atalar, H. Koymen, "Parametric Nonlinear Lumped Element Model for Circular CMUTs in Collapsed Mode" , IEEE Transactions on Ultrasonics, Ferroelectrics, and Frequency Control, January 2014.

©2013 IEEE. Reprinted, with permission, from E. Aydogdu, A. Ozgurluk, H. K. Oguz, A. Atalar, H. Koymen, "Lumped Element Model of Single CMUT in Collapsed Mode" , IEEE International Ultrasonics Symposium, July 2013.

©2012 IEEE. Reprinted, with permission, from E. Aydogdu, A. Ozgurluk, H. K. Oguz, A. Atalar, C. Kocabas, H. Koymen, "Nonlinear Equivalent Circuit Model for Circular CMUTs in Uncollapsed and Collapsed Mode" , IEEE International Ultrasonics Symposium, October 2012.

ABSTRACT

LUMPED ELEMENT MODELING OF CIRCULAR CMUT IN COLLAPSED MODE

Elif Aydoğdu
Ph.D. in Electrical and Electronics Engineering
Advisor: Prof. Dr. Abdullah Atalar
Co-Advisor: Prof. Dr. Hayrettin Köymen
January, 2014

Capacitive micromachined ultrasonic transducer is a microelectromechanical device, which serves as an acoustic signal source or sensor, in a variety of applications including medical ultrasound imaging, ultrasound therapy, airborne applications. It has a suspended membrane with an electrode inside, and at the underlying substrate there is another electrode, so that the membrane can be deflected by the electrical field formed between the electrodes. Similarly, any mechanical disturbance on the membrane can be sensed as a change in the capacitance of the two electrodes.

CMUT is a nonlinear device which has a distributed mechanical operation. Although, it is a mass-spring system basically, the nonlinear electrical force and the radiation force makes it impossible to solve CMUT through analytical equations. In order to predict its behavior, and design a CMUT towards the needs of a specific application, either finite element analysis or equivalent electrical circuit modeling should be utilized. Finite element analysis (FEA) can predict the distributed CMUT operation with high accuracy, but its usage is limited to designs employing low number of CMUTs because of the computation cost. Recently, advances in equivalent circuit modeling, made it possible to simulate arrays employing very high number of CMUTs, with high accuracy. These models assume uncollapsed mode operation and except collapsed mode operation as it is highly nonlinear.

This thesis focuses on obtaining an accurate equivalent circuit model for a circular CMUT in collapsed mode. The outcome is a parametric circuit model, that can simulate a CMUT of any physical and material parameters, under an arbitrary electrical or mechanical excitation. In collapsed mode, the compliance

of the membrane is no longer constant as in uncollapsed mode, and it increases with increasing contact radius. Similarly, the capacitance, the electrical force and the radiation impedance all have new behavior regarding the contact radius. As there is no analytical solution for those parameters, we perform numerical calculations and extract expressions for each of them.

First, we calculate the collapsed membrane deflection, utilizing the exact electrical force distribution in the analytical formulation of membrane deflection. Then we use the deflection profile to calculate the capacitance, electrical force, and compliance. Performing a set of calculations for different CMUT dimensions, different pressure and voltage levels, we obtain dependencies of those parameters on rms deflection. Then we develop a lumped element model of collapsed membrane operation, expressing the parameters as functions of rms deflection. The radiation impedance for the collapsed mode is also included in the model. The model is then merged with the uncollapsed mode model to obtain a simulation tool that handles all CMUT behavior, in transmit or receive. Large- and small-signal operation of a single CMUT can be fully simulated for any excitation regime. The results are in good agreement with FEM simulations.

Keywords: Capacitive Micromachined Ultrasonic Transducers, Circular CMUT, MEMS, Lumped Element Model, Equivalent Circuit Model, Collapsed Mode, Collapsed CMUT Array, Collapsed Mode Radiation Impedance.

ÖZET

DAİRESEL CMUT İÇİN ÇÖKME MODU EŞDEĞER DEVRE MODELİ

Elif Aydoğdu
Elektrik Elektronik Mühendisliği, Doktora
Tez Danışmanı: Prof. Dr. Abdullah Atalar
Tez Eş Danışmanı: Prof. Dr. Hayrettin Köymen
Ocak, 2014

Kapasitif mikroişlenmiş ultrasonik çevirici (CMUT), ultrasonik görüntüleme, ultrason terapisi, havada uygulamalar başta olmak üzere pek cok uygulamada akustik kaynak ve algılayıcı olarak gelecek vaadeden bir mikroelektromekanik yapıdır. Havada asılı bir membrana yerleştirilmiş bir elektrod ile altındaki zeminde serili bir elektroddan oluşmaktadır ve bu sayede iki elektrod arasında elektrik alan oluşturularak membranın bükülmesi sağlanmaktadır. Benzer şekilde, membranı hareket ettiren herhangi bir kuvvet elektrodlar arasındaki kapasitansta bir değişim olarak algılanabilmektedir.

CMUT, lineer olmayan ve uzayda yayılmış hareketi olan bir cihazdır. Mekaniği, basit anlamda bir yay-kütle sistemi olsa da, üzerindeki elektrik kuvvetin ve radyasyon empedansının lineer olmaması, analitik denklemlerle çözülmesini engellemektedir. Bir uygulamanın gereksinimlerine dönük tasarım yaparken, CMUT davranışını simüle edebilmek için FEA (sonlu eleman analizi) ya da eşdeğer devre modeli kullanılmaktadır. FEA simulasyonları, CMUT'ın uzayda yayılmış davranışını yüksek doğrulukla öngörebilmektedir, ancak işlem yükünün çok fazla olması bu yöntemin sadece birkaç CMUT'ı modellemek için kullanılmasına izin vermektedir. Son yıllarda gelişmeler kaydedilen eşdeğer devre modeli çalışmaları, binlerce CMUT içeren dizilerin bile yüksek doğrulukla modellenmesine imkan sağlamıştır. Bu modeller, çökme öncesi modda CMUT lar için kullanılmakta, yüksek nonlineeriteye sahip çökme modunu içermemektedirler.

Bu tez, çökme modunda CMUTlar için yüksek doğruluğu olan bir eşdeğer devre modeli oluşturulmasını amaçlamaktadır. Tezin çıktısı, herhangi bir fiziksel ve maddesel parametre setine sahip bir CMUT'ın rastgele bir sinyalle sürülmesinin simüle edilebildiği, parametrik bir eşdeğer devre modelidir. Çökme modunda,

membranın yay sabiti çökme öncesi moddaki gibi sabit değildir ve artan çökme yarıçapıyla birlikte artmaktadır. Benzer şekilde, kapasitans, elektriksel kuvvet ve radyasyon empedansı da çökme öncesi moddan farklı davranışa sahiptir. Bu parametrelerin hiçbiri için analitik bir formulasyon yapılamadığı için, herbiri numerik hesaplamalar sonucunda formulize edilmektedir. Modelleme prosedürü şu şekilde özetlenebilir:

Öncelikle, çökme modunda membran profilini, gerçek elektriksel kuvvet dağılımını kullanarak hesaplıyoruz. Ardından bu profili kullanarak, kapasitansı, elektriksel kuvveti ve yay sabitini buluyoruz. Farklı pek çok CMUT boyutunda, farklı basınç ve voltaj seviyeleri için bu hesaplamaları gerçekleştirerek, herbir parametrenin rms çökme değerine bağlı davranışını ortaya çıkarıyoruz. Sonra bu parametreleri rms çökmenin fonksiyonu olarak ifade ederek, eşdeğer devre modelini oluşturuyoruz. Modeli çökme modundaki CMUTlar için hesaplanmış radyasyon empedansını kullanarak tamamlıyoruz. Ayrıca modeli, çökme öncesi mod modeliyle bütünleştirerek, CMUT davranışını kapsayan tek bir model elde ediyoruz. Bu modelle, CMUTın alıcı ve verici olarak, küçük ve büyük sinyal operasyonları, herhangi bir sürme rejiminde simule edilebilmektedir. Elde ettiğimiz sonuçlar, FEA sonuçlarıyla uyumlu olmuştur.

Anahtar sözcükler: Kapasitif Mikroişlenmiş Ultrasonik Çeviriciler, Dairesel CMUT, MEMS, Toplu ögeli model, Eşdeğer devre modeli, Çökme modu, Çökme modunda CMUT dizisi, Çökme modunda radyasyon empedansı.

Acknowledgement

I owe my deepest gratitudes to my supervisors Professor Hayrettin Köymen and Professor Abdullah Atalar. I have always felt very fortunate to be enlightened by their wisdom and looked up to them. Prof. Atalar has always patiently guided me through rough steps since I was an undergraduate student. It was a pleasure and honor to get exposed to his extensive knowledge and experience, and learn how to consider problems from various aspects. In 2011, I started closely working with Prof. Köymen, his vast amount of knowledge and foreseeing genius taught me a lot. I gained a wider engineering perspective thanks to him. He has always generously supported and mentored us through all aspects of life. His belief in me, which made me a confident engineer, is very valuable to me. I will always feel sincerely indebted to Prof. Köymen and Prof. Atalar for their endless encouragement.

I would like to thank Professor Ergin Atalar for his guidance in my early Ph.D. studies. I learned a lot from him, and gained useful knowledge on MRI. I also would like to thank Professor Atilla Aydınlı for his support in my graduate life, and his friendly mentoring. He has always increased my enthusiasm in science since my first Bilkent day in his Physics 101 class. I thank Prof. Atalar, Prof. Aydınlı, and Assoc. Prof. A. Sanlı Ergün, and Asst. Prof. Coşkun Kocabaş for their useful feedback throughout my studies.

I would like express my gratitudes to TÜBİTAK for the financial support (2211 scholarship program) I received during my graduate research. I also studied under the project grant 110E216 of TÜBİTAK.

There are many precious people in Bilkent, who are like a family to me. I will be missing Mürüvet Parlakay, Ergün Hırlakoğlu, Ersin Başar, Aydan Ercingöz, and Ebru Ateş. Also, I owe much to Murat Güre, and Ergün Karaman.

My colleagues Aslı Ünlügedik, Niyazi Şenlik, Selim Olçum, Kağan Oğuz, Sinan Taşdelen, Ceyhun Kelleci, Yasin Kumru, Yavuz Kansu, and Burak Şahinbaş are all valuable friends to me. Aslı and me have shared a lot of fun moments; travels, discoveries, conferences; and also companied each other in many stressful times. Niyazi usually made things harder with his point of view, but still I feel lucky to have his friendship. Selim has been a third advisor to me, I benefited a lot from his knowledge, he and Kağan have always generously helped at every stage of this work. Yasin and Burak have always made me smile with their positiveness. In the end, I am grateful to all of them for making Ph.D. studies easier. I also sincerely thank Alper Özgürlük, for his contribution to this thesis.

Bilkent has brought me many excellent lifelong friends, Emre Kopanoğlu-brother, Kıvanc Köse, Can Uran, Can Kerse, Esra Abacı, Bora Esmer, Celal Alp Tunç, Alexander Suhre, Alican Bozkurt, Ayça Özçelikkale, Mehmet Köseoğlu, Mohammad Tofighi -the list is actually much longer. We had wonderful memories at Bilkent. I am grateful to them, for all those beautiful times we had together.

Finally, I am deeply indebted to my Gökçe (Aksoy), Özge (Öztürk), Selen (Pehlivan), Gülis (Zengin), İlknur (Tunç), Özgül (Pekcan) (in the order we first met) being next to me every moment I needed, they have a special place in my heart. I also owe thanks to Selen, Özgül, Yasin and Alican for their generous help in my last and most stressful Ph.D. days.

I dedicate this thesis to my grandmother, who is my angel, and to my large and warm hearted family. No words can express my gratitude to them, I walked through all the obstacles in my life, with their love and endless support.

Contents

List of Figures

List of Tables

Chapter 1

Introduction

Capacitive micromachined ultrasonic transducer is an electromechanical device, which has a suspended membrane and two electrodes, one deposited inside the membrane and the other lying on the substrate underneath. Applying an electrical signal across the two electrodes, an electrical field is obtained on the membrane; and controlling the applied signal, the membrane can be vibrated at a specific frequency and amplitude as an acoustic source. Also as a sound and force sensor, an external mechanical excitation will alter the capacitance between the electrodes, creating a signal at the electrical port.

This electrically controlled acoustic device can be used towards various purposes including medical ultrasound imaging [1–9], ultrasonic therapeutics [10], and airborne applications [11–13]. CMUT is a promising technology for each of the given applications, with its low fabrication cost, CMOS compatibility [14–17], modularity, and large bandwidth. However, it has no widespread commercial usage yet, since it is a highly nonlinear device, and its operation characteristics have not yet been fully uncovered since its invention in 1990s [18]. Especially, in arrays, CMUTs tend to have unexpected resonances due to crosstalk [19], and designing a CMUT array is a difficult process.

Accurate modeling of capacitive micromachined ultrasonic transducers (CMUTs) is essential to avoid long trial and error cycles in CMUT design and manufacturing. As a CMUT's mechanical operation is distributed and nonlinear, its modeling is not straightforward. There have been several approaches reported in the literature. The most reliable, and a very commonly used method has been finite element analysis (FEA) [20–23]. In the finite element analysis environment, the distributed operation of a CMUT membrane can be simulated with high accuracy at the cost of extensive computation and time consumption. It is possible to use symmetry properties and model only a portion of a single CMUT or a symmetrical CMUT array to decrease the computation cost, but this only helps to simulate either infinitely long arrays which is not realistic but only an approximation, or small arrays of less than ten CMUTs. Also, FEA is not practical as transient or harmonic analysis of even a single CMUT lasts a day, and the computation cost exponentially increases with increasing cell count. This forces researchers to use alternative methods for predicting CMUT operation. The methods include characterization of CMUT behavior using experimental observations [24–26], analytical calculation of the distributed membrane bending and the electrical-mechanical energy transfer efficiency [27–30], and defining lumped elements to develop models suitable for dynamic simulations. Electrical circuit elements constitute a convenient basis for CMUT modeling. Starting from Mason's model for acoustic transducers [31], equivalent circuit modeling has been improving as a powerful alternative to FEA [18, 28, 32–35], especially for array modeling [36–38]. The studies directed toward understanding and modeling mutual impedance of CMUT arrays [19, 23, 25, 38–41] have helped to improve the accuracy of lumped element simulations.

Currently, the uncollapsed mode operation of CMUT arrays is well understood through equivalent circuit model simulations [38, 42, 43]. The mechanical and electrical properties of uncollapsed mode operation are perfectly adapted to the lumped model [35]. A significant phenomenon that should be handled in CMUT design process is the crosstalk of CMUTs in arrays. Lumped element modeling turns out to be very successful also at predicting crosstalk effects [38] by including mutual radiation impedance between each cell pair. CMUTs are commonly used in large arrays, and currently lumped element modeling is the accurate and the only way of predicting the operation of large CMUT arrays.

The missing part in the developed lumped element models is the collapsed mode operation; CMUT operation beyond the collapse point cannot be simulated. Even in the arrays, that are driven in uncollapsed mode, some of the CMUTs may experience collapse due to mutual radiation impedance. However, collapsed mode was left out of the models, as its operation is highly nonlinear and all the lumped elements should be redefined in this mode. In collapsed mode, it is not possible to obtain analytical expressions for the lumped deflection, velocity, capacitance, electrical force, membrane compliance and also radiation impedance. This makes it very difficult to analyze this mode.

Collapsed mode offers high transmit efficiency as given in [44–48]. In [48], uncollapsed and collapsed modes are compared, and it is concluded that a CMUT can produce much higher transmit power in deep collapse mode than that in uncollapsed mode. As the membrane is in contact with the insulating layer, the effective gap height is smaller and larger electrical force can be obtained with the same voltage. At the same time, the membrane stiffness increases with increasing contact radius, which makes it possible to store more energy on the membrane and release at transmit. In order to explore this mode further, it is necessary to obtain a lumped element model. An equivalent circuit model for collapsed mode was previously introduced in [49]. However, it was not a fully parametric model. Numerical calculations of the bending profile of a specific CMUT design were adapted to the model; hence, new numerical calculations had to be carried out for every new set of design parameters. Also, the bending profile calculations were done utilizing Timoshenko's [50] uniform force solution, and this uniformity approximation did not result in high accuracy.

In this work, a fully parametric model for a CMUT in collapsed mode is obtained. First, the collapsed membrane bending is calculated with high accuracy, utilizing the non-uniform electrostatic force expression in Timoshenko's equation instead of the uniform force approximation. The bending profile is used to calculate the rms displacement and capacitance. The calculations are then adapted to the lumped element model of [35], and the electrical force and compliance expressions are obtained. We model the collapsed mode operation of CMUT close to FEM accuracy, including the self and mutual radiation impedance of collapsed mode [51]. We also merge the model with the uncollapsed mode part given in [37] and obtain a single model for the entire large-signal operation of the CMUT.

Chapter 2

Calculation of Bending Profile in Collapsed Mode

2.1 Accurate Formulation of Deflection-Force Relation

In this thesis, we are interested in modeling collapsed mode CMUTs with circularly clamped membranes. Fig. 2.1 shows the profile of a CMUT cell in the collapsed mode, while Table 2.1 lists the description of relevant variables.

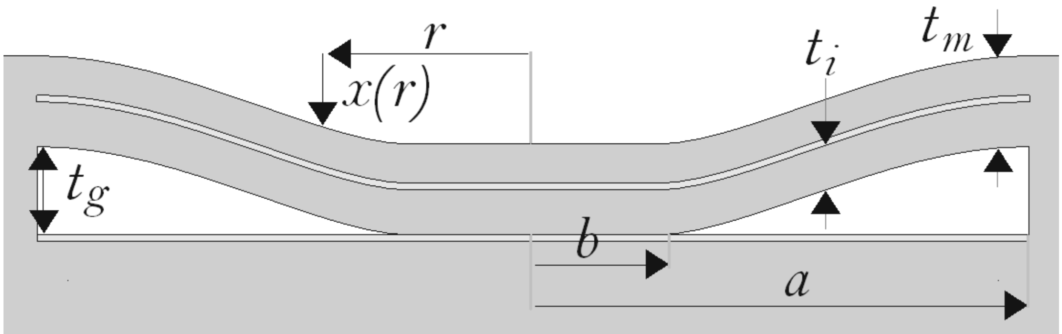

Figure 2.1: The dimensional parameters of a CMUT in collapsed mode

We assume the loading on the membrane is circularly symmetrical, and so is

Table 2.1: Description of parameters

a	membrane radius
b	contact radius in case of collapse
$x(r)$	displacement profile
ϵ_0	dielectric permittivity of air
ϵ_r	relative dielectric permittivity of insulator
t_g	gap height
t_i	insulator thickness
t_{ge}	effective gap height: $t_{ge} = t_g + t_i/\epsilon_r$
t_m	membrane thickness
E	Young's modulus of membrane material
υ	Poisson's ratio of membrane material
ρ	density of membrane material
D	flexural rigidity of membrane material
ρ_0	density of immersion medium
c_0	speed of sound in immersion medium

the membrane bending. Timoshenko provides the calculation of bending profile for symmetrical load distribution on circular plate in [50], page 54,

$$\frac{d}{dr}\left(\frac{1}{r}\frac{d}{dr}\left(r\frac{d\,x(r)}{dr}\right)\right) = \frac{Q(r)}{D}. \tag{2.1}$$

In this equation, $Q(r)$ is the shearing force at radius r, $x(r)$ is the bending amount at r, b is the contact radius, and $D = E\,t_m^3/12\,(1-\upsilon^2)$ is the flexural rigidity (a physical parameter). $Q(r)$ is equal to the load within the circle of radius r, divided by $2\pi r$:

$$Q(r)\,2\pi r = \int_b^r P(\xi)\,2\pi\xi\,d\xi. \tag{2.2}$$

$P(r)$ is the force density distribution. It includes all the forces acting on the membrane, which are the ambient pressure, the electrical force, the inertial force of the membrane mass, and the force due to medium loading. Replacing $Q(r)$, we end up with the following equation relating the bending profile, $x(r)$, to $P(r)$:

$$r\frac{d}{dr}\left(\frac{1}{r}\frac{d}{dr}\left(r\frac{d\,x(r)}{dr}\right)\right) = \frac{1}{D}\int_b^r P(\xi)\xi\,d\xi \tag{2.3}$$

The electrical force density distribution on the membrane can be expressed with the following equation:

$$P_E(r) = \frac{\epsilon_0\,V^2}{2\,(t_{ge} - x(r))^2} \tag{2.4}$$

The electrical force density is the electrostatic force on the unit area capacitor with a gap $t_{ge} - x(r)$, having a voltage V across it. This expression is highly nonlinear, and if $P(r)$ is expressed as the summation of the electrical force and the other forces, $x(r)$ cannot be solved analytically.

A convenient approach for calculation of uncollapsed membrane bending is to approximate all forces with an equivalent uniform pressure distribution across the membrane. This way, $x(r)$ can be expressed analytically as

$$x(r) = x_p\left(1 - \frac{r^2}{a^2}\right)^2 \quad ,\ (x_p\text{: peak displacement}) \tag{2.5}$$

and moreover this deflection formula can be used to obtain analytical expressions for lumped, electrical force, capacitance, and mechanical compliance. So, uniform pressure approximation is commonly used for formulating the uncollapsed mode operation, in which the electrical force distribution on the membrane is almost uniform.

In the collapsed mode, if all the forces are approximated with an equivalent uniform pressure, the deflection profile can be expressed in the following form:

$$x(r) = C_1 + C_2\,r^2 + C_3\,\log(r) + C_4\,r^2\,\log(r) + C_5\,r^4 \tag{2.6}$$

(C_1, C_2, C_3, C_4 and C_5 are constants)

However, this uniform pressure approximation does not yield accurate results for a collapsed membrane, as the electrical force distribution is highly nonuniform in collapsed mode. In collapsed mode, the center of the membrane is in contact with the insulating layer, and the effective gap height is very small in this contact region. In previous studies [49], it was observed that the calculated contact radius turns out to be smaller than expected when the force distribution on the membrane is assumed to be uniform. In reality, the electrical force increases significantly close to the contact point because of the decreased gap, exerting a higher pulling force in this region compared to the periphery (Fig.2.2).

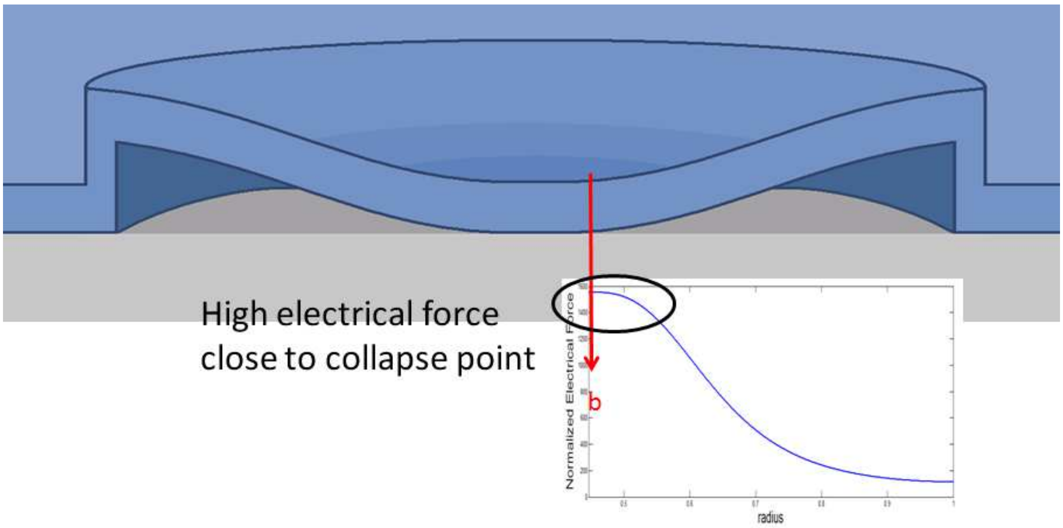

Figure 2.2: The force density distribution beyond contact point

As a result there is increased bending at that region. This effect is shown in Fig.2.3. The upper plot shows the bending profile calculated with uniform force approximation, and the lower plot is the bending profile obtained with the electrical force distribution. We observe that the contact radius is larger than the prediction of uniform force calculations, and the two bending profiles are different.

In our calculations, instead of uniform pressure approximation, we utilize the combination of uniformly distributed forces and electrical force density, which we call the *model* force, in Timoshenko's equation:

$$r\frac{d}{dr}\left(\frac{1}{r}\frac{d}{dr}\left(r\frac{d}{dr}x(r)\right)\right) = \frac{1}{D}\int_b^r \left(P_b + \frac{\epsilon_0 V^2}{2\,(t_{ge} - x(\xi))^2}\right)\xi d\xi. \qquad (2.7)$$

Here, the pressure term $P(r)$ is replaced with the electrical force density at every point on the membrane, added to the remaining uniformly distributed static pressure P_b. P_b accounts for the ambient atmospheric or hydrostatic pressure. t_{ge} is the effective gap height with $t_{ge} = t_g + t_i/\epsilon_r$ where t_g is the gap height, t_i is the

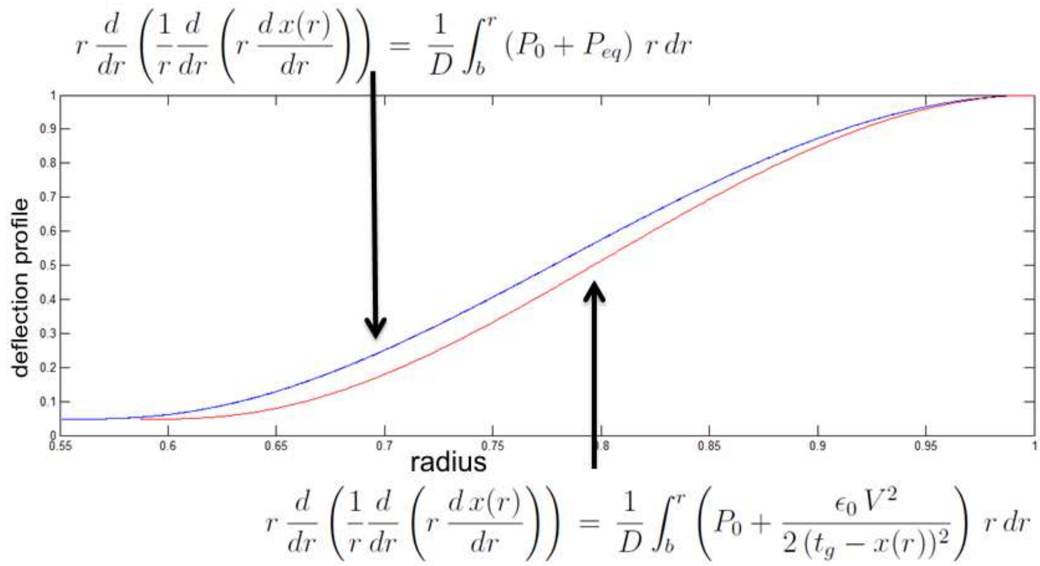

Figure 2.3: Deflection profile obtained using electrical force density(lower curve), compared to the one calculated by the uniform-force approximation (upper curve)

insulator thickness, and ϵ_r is the relative dielectric permittivity of the insulator as given in Table 2.1.

There is no analytical solution for $x(r)$ of (2.7), and it needs to be solved numerically. This means we have to perform the numerical calculations for every possible CMUT design of different physical and material parameters, under different static pressure and excitation voltage combinations. This requires very large number of calculations to obtain a database and form a general model. However, there is a way to achieve this with much less calculations; all the parameters can be normalized to a basis and the calculations can be carried out in this basis. The procedure is described below.

We first normalize the variables and rearrange (2.7) into the generic form

$$\overline{r}\frac{d}{d\overline{r}}\left(\frac{1}{\overline{r}}\frac{d}{d\overline{r}}\left(\overline{r}\frac{d}{d\overline{r}}\overline{x}(\overline{r})\right)\right) = \int_{\overline{b}}^{\overline{r}} 64\left(\frac{P_b}{P_g} + \frac{2\,(V/V_r)^2}{9(1-\overline{x}(\xi))^2}\right)\xi d\xi \tag{2.8}$$

where the normalized variables are

$$\overline{r} = \frac{r}{a}, \quad \overline{b} = \frac{b}{a}, \quad \overline{x}(.) = \frac{x(.)}{t_{ge}}. \tag{2.9}$$

P_g is the pressure that corresponds to a peak membrane displacement of t_{ge} at zero bias ($\overline{x}(0) = 1$), and V_r is the collapse voltage at vacuum [35]:

$$P_g = \frac{64\, D\, t_{ge}}{a^4}, \quad V_r = \frac{16}{3\, a^2}\sqrt{\frac{D\, t_{ge}^3}{\epsilon_0}}. \tag{2.10}$$

The boundary conditions of the differential equation in (2.8) can be written as

$$\begin{aligned} \overline{x}(\overline{r})|_{\overline{r}=1} = 0, \qquad \overline{x}(\overline{r})|_{\overline{r}=\overline{b}} = \frac{t_g}{t_{ge}}, \qquad \left.\frac{d}{d\overline{r}}\overline{x}(\overline{r})\right|_{\overline{r}=1} = 0, \\ \left.\frac{d}{d\overline{r}}\overline{x}(\overline{r})\right|_{\overline{r}=\overline{b}} = 0, \quad \left.\frac{d^2}{d\overline{r}^2}\overline{x}(\overline{r})\right|_{\overline{r}=\overline{b}} = 0. \end{aligned} \tag{2.11}$$

The input parameters are V/V_r, P_b/P_g, and t_g/t_{ge}. The resulting $\overline{b}$ and $\overline{x}(\overline{r})$ are calculated using the algorithm described in the following section. Using this algorithm, we obtain a set of normalized results, and this set can be used to find the bending profile of any CMUT through simple arithmetical calculations.

2.2 Solution Algorithm

Our strategy of solving (2.8) under the boundary conditions of (2.11) is expressing the force term in such a way that an analytical solution can be obtained. If the pressure term can be expressed as a Kth degree polynomial as in the following equation

$$\overline{r}\frac{d}{d\overline{r}}\left(\frac{1}{\overline{r}}\frac{d}{d\overline{r}}\left(\overline{r}\frac{d}{d\overline{r}}\overline{x}(\overline{r})\right)\right) = \int_{\overline{b}}^{\overline{r}}\left(\sum_{n=1}^{K} c_n\, \xi^n\right) d\xi \tag{2.12}$$

an analytical solution exists

$$\begin{aligned} \overline{x}(\overline{r}) = A_1 + A_2\,\overline{r}^2 + A_3\, \log(\overline{r}) + A_4\,\overline{r}^2\, \log(\overline{r}) \\ + \sum_{n=1}^{K}\frac{c_n\,\overline{r}^{n+3}}{(n+1)^2(n+3)^2} \\ + \overline{r}^2\,(1 - \log(\overline{r}))\sum_{n=1}^{K}\frac{c_n\,\overline{b}^{n+1}}{4(n+1)} \end{aligned} \tag{2.13}$$

where A_1, A_2, A_3, and A_4 are the constants of integration.

We use (2.13) in our iterative solution routine as demonstrated in Fig. 2.4 and explained below:

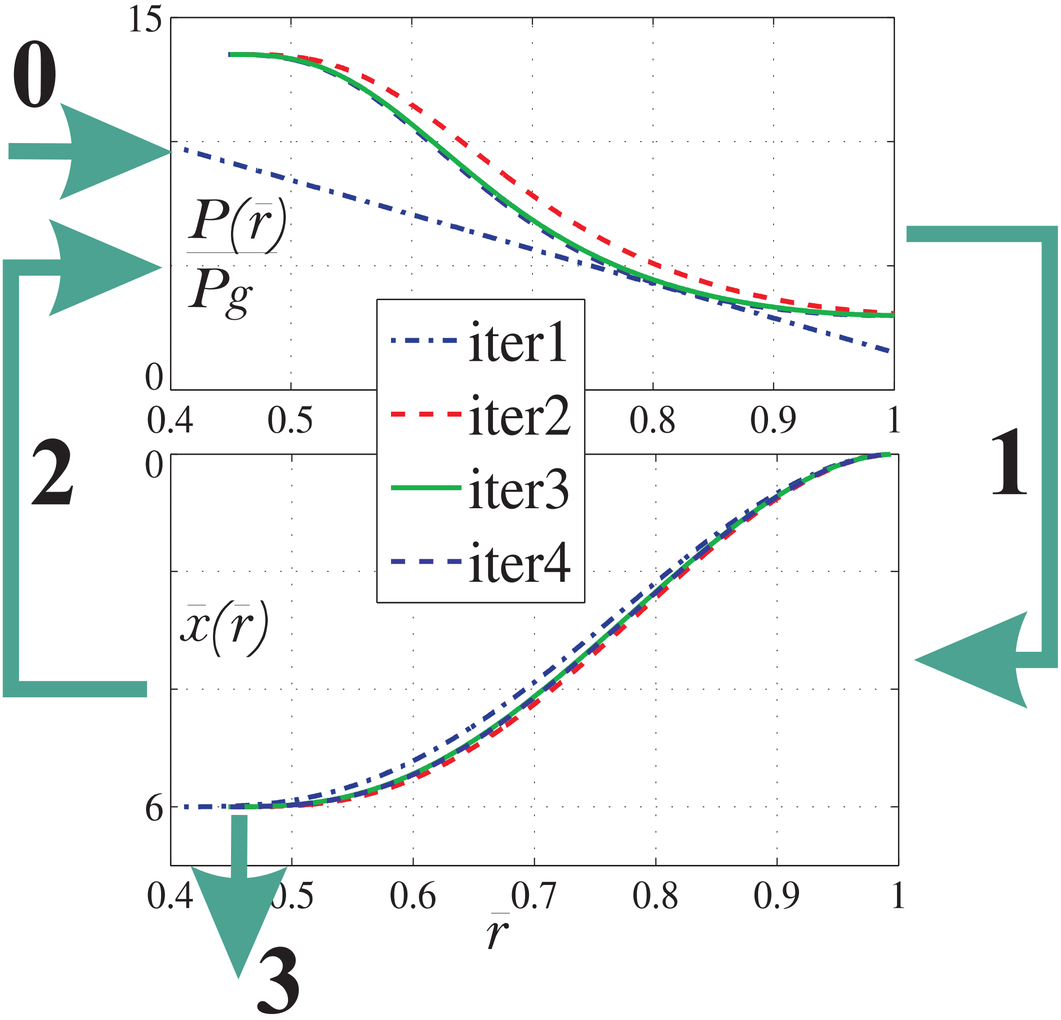

Figure 2.4: Demonstration of iterative algorithm for solving $\overline{x}(\overline{r})$

0. Given the physical parameters, the normalized static force, and the excitation voltage, start with an initial guess of the pressure distribution. To enable faster convergence, the following linearly varying pressure distribution is used as the initial guess[1]:

$$\frac{P(\overline{r})}{P_g} = \frac{P_b}{P_g} + 1.5\frac{2\,(V/V_r)^2\,(1-\overline{r})}{9(1-t_g/t_{ge})^2} \tag{2.14}$$

[1]The initial pressure should be sufficiently high to make the membrane collapse.

1. A polynomial with coefficients c_n $(n = 0, 1, \ldots K)$ is fitted to the pressure distribution. To achieve convergence in all cases, we set $K = 14$. Substituting this polynomial into (2.12), an analytical expression for $\overline{x}(\overline{r})$ in (2.13) with five unknowns (A_1, A_2, A_3, A_4 and $\overline{b}$) is obtained. The first four boundary conditions in (2.11) are solved with a symbolic math package to express A_i in terms of $\overline{b}$. Then, the last boundary condition is used to determine $\overline{b}$ by finding the zero crossing point.

2. Using the obtained bending profile, $\overline{x}(\overline{r})$, the new pressure distribution is calculated through the electrical force density expression in the right-hand side of (2.8):

$$\frac{P(\overline{r})}{P_g} = \frac{P_b}{P_g} + \frac{2\,(V/V_r)^2}{9(1-\overline{x}(r))^2}$$

3. Go to step **1** and repeat until $\overline{b}$ convergences to a value within $\simeq 0.1\%$ difference between successive iterations.

In this routine, it is challenging to have convergence for all cases. In the application of the routine, the force polynomial fitting process should be carefully handled considering the next iteration step, in order to avoid very high force at the contact radius of the next iteration, and ensure convergence. The MATLAB code is given and described in detail in the Appendix.

Plots for $\overline{x}(\overline{r})$ calculations are given in Fig. 2.5, showing the difference between the bending profiles obtained with uniform pressure approximation, and *model* force with $P_b = 0$. There are four cases for a CMUT of $t_g/t_{ge} = 0.9$. In the uncollapsed mode, close to the collapse point, where $\overline{x}_P = \overline{x}(0) = 0.45$ (normalized *peak* displacement), the two profiles are very similar. This means the uniform pressure approximation can be used for predicting uncollapsed mode operation. However, as the displacement increases and the membrane enters the unstable region, the profiles start to diverge from each other, as seen in the $\overline{x}_P = 0.7$ plot. At the snapback point where the membrane barely touches bottom, and in the collapsed mode, the difference is even larger. At snapback, the uniform pressure approximation gives $V = 0.55V_r$ and $\overline{x}_R = 0.402$ (normalized *rms* displacement[2]),

[2]This is defined by $\overline{x}_R = \sqrt{1/(\pi a^2)\int_0^a 2\pi r \overline{x}^2(r)dr}$.

while the *model* force results in $V = 0.58V_r$ and $\overline{x}_R = 0.358$.

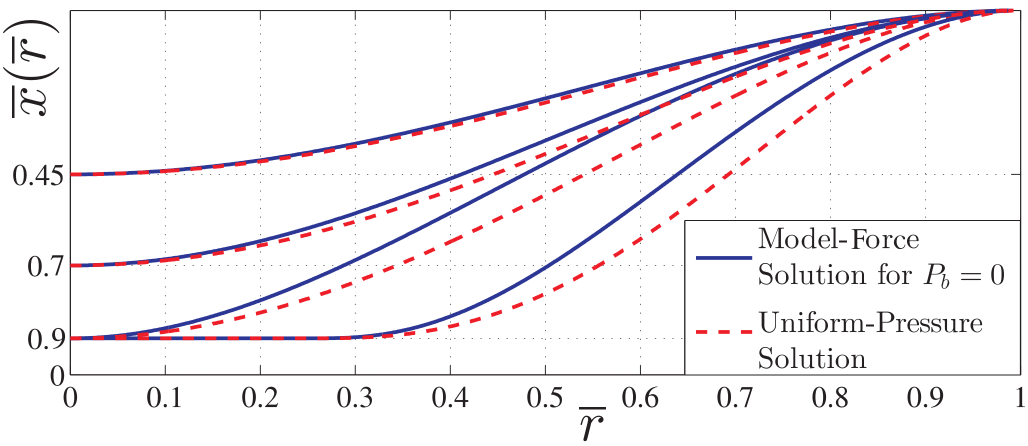

Figure 2.5: Normalized deflection profiles of uniform pressure-loaded ($V = 0$) and *model* force-loaded ($P_b = 0$) membranes with $t_g/t_{ge} = 0.9$. Both profiles have the same peak displacements ($\overline{x}_P = 0.45$ and 0.7) in uncollapsed mode, and the same contact radius at snapback ($\overline{b} = 0$) and in collapsed mode ($\overline{b} = 0.25$).

2.3 Results: Collapse and Snapback

The transduction force, the capacitance and the compliance of CMUT are determined by the deflection profile. The profile depends both on the normalized static pressure, which is uniformly distributed, and on the electrical force. In the model presented in this thesis, the effect of the profile is uniquely summarized in rms displacement. Although one can have the same rms displacement for different combinations of normalized static ambient pressure and electrical force, for a given pair of P_b/P_g and t_g/t_{ge}, the electrical force and the model elements can be uniquely defined as functions of rms displacement.

In Fig. 2.6, the applied normalized bias voltage is plotted versus normalized rms displacement as a continuation of the CMUT biasing chart of [35] at $P_b/P_g = 0.2$ (dotted). Static deflection profiles obtained at $P_b/P_g = 0.2$ and t_g/t_{ge}= 0.4, 0.5, 0.6, 0.65, 0.73, 0.9, for V/V_r<10 are used to calculate the rms displacement ($\overline{x}_R = x_R/t_{ge}$) of each profile. In the collapsed mode, the displacement-voltage relationship changes with changing t_g/t_{ge} value.

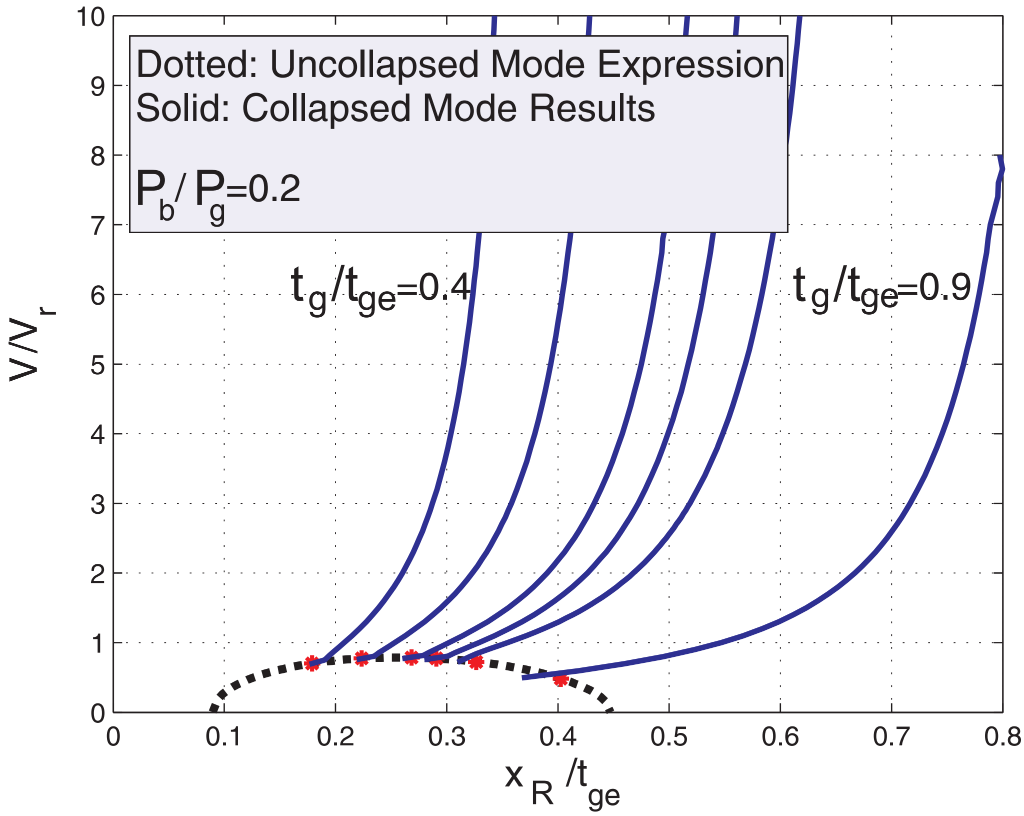

Figure 2.6: CMUT biasing chart covering uncollapsed and collapsed regions at $P_b/P_g = 0.2$, and t_g/t_{ge}=0.4, 0.5, 0.6, 0.65, 0.73, 0.9

In order to see the difference, the snapback points (where the membrane releases from the bottom layer) obtained with our calculations, and uniform-force calculations are closely plotted in Fig. 2.7. Blue dots show the correct snapback points obtained with *model* force calculations, while red dots on the dashed line are the uniform force assumption solutions. We observe that the uniform-force solution brings significant error especially for larger t_g/t_{ge}, where the electrical force is highly nonuniform.

In Fig. 2.8, rms displacements calculated with both the *model* force and the uniform force approximation are plotted as a function of normalized bias voltage, at $P_b/P_g = 0$ and $t_g/t_{ge} = 0.73$. The uncollapsed mode static analysis result for vacuum ($P_b = 0$), obtained with the uniform pressure approximation given in Fig. 5 of [35] is shown here with a dashed curve. The *model* force result

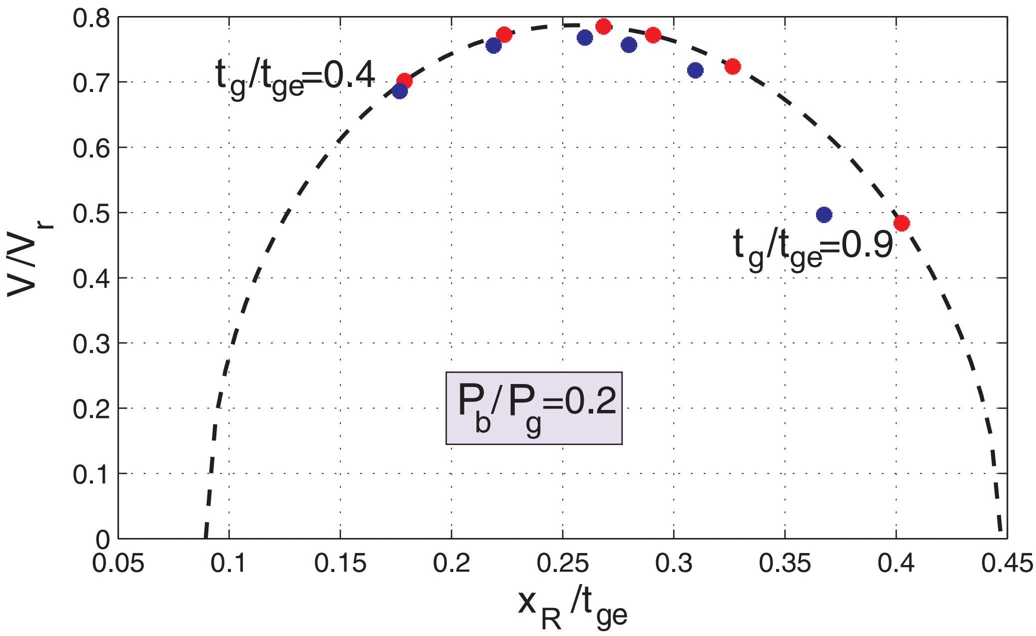

Figure 2.7: Snapback points for t_g/t_{ge}=0.4, 0.5, 0.6, 0.65, 0.73, 0.9 on CMUT biasing chart at $P_b/P_g = 0.2$. Red dots on the dashed line are the uniform pressure approximation solutions. Separate blue dots are calculated with actual force profile

shown in the plot (solid curve) is obtained also in vacuum, and the electrical force distribution on the membrane is highly non-uniform in the unstable region and in the collapsed region. The results obtained with the uniform pressure approximation of electrical force (Eq.2.6) considerably diverge from the *model* force results in these regions. This is the source of the error in the prediction of snapback voltage in [49].

The transition from the uncollapsed mode to the collapsed mode happens at a voltage level where the membrane quickly passes through the unstable region and reaches a new balance point in the collapsed region (upward arrow). The snapback transition from the collapsed mode (at zero contact radius) to the uncollapsed mode occurs at a lower voltage (downward arrow).

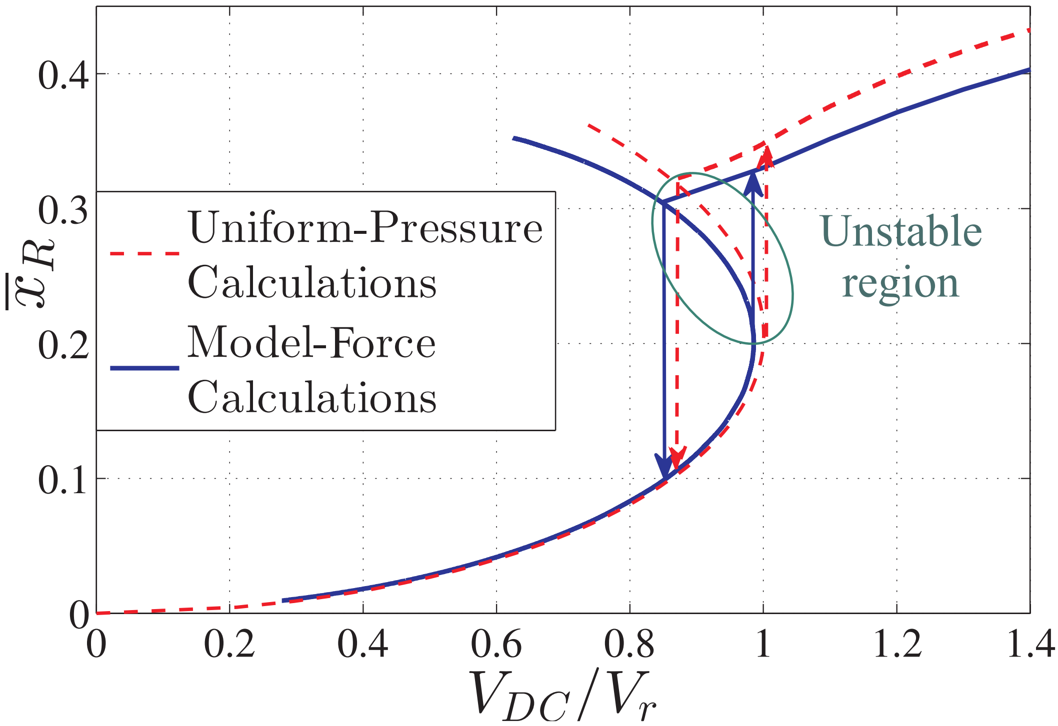

Figure 2.8: Normalized displacement $\overline{x}_R$ as a function of normalized applied voltage V_{DC}/V_r in uncollapsed and collapsed modes for $t_g/t_{ge} = 0.73$.

Chapter 3

Lumped Element Model of a Single CMUT in Collapsed Mode

The static calculations of collapsed membrane bending are used to define the elements in the lumped model of Fig. 3.1. As seen from the electrical side, the

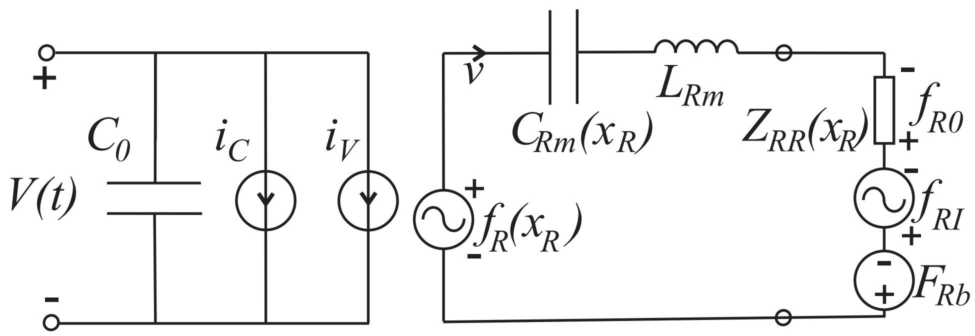

Figure 3.1: The equivalent electrical circuit model of a CMUT with the through variable v_R.

CMUT behaves like a capacitor whose value depends on instantaneous membrane displacement. On the left side of Fig. 3.1, this is represented with C_0, the undeflected membrane capacitance, and two current sources, i_C and i_V [35]

$$i_C = (C - C_0)\frac{dV(t)}{dt} \tag{3.1}$$

$$i_V = V(t)\frac{dC}{dt} \tag{3.2}$$

where C is the instantaneous electrical capacitance.

In the electrical analogy of CMUT mechanics, the through and across variables are the rms velocity v_R and the corresponding energy-conserving rms force f_R [35]. On the right side of Fig. 3.1, we see the rms forces acting on the membrane: the electrical force f_R, the force due to ambient pressure F_{Rb}, and the dynamic external force f_{RI} (Fig.3.2). Another force is the inertial force of the membrane mass. The membrane exerts a restoring force against all forces, determined by its

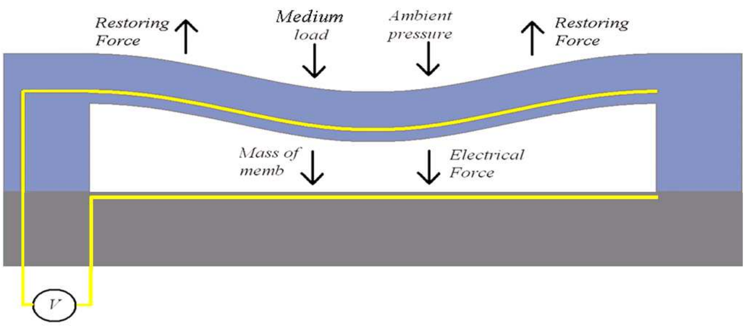

Figure 3.2: The forces acting on the CMUT membrane.

compliance C_{Rm}. In the uncollapsed mode, the compliance has a fixed value [35] of

$$C_{Rm_0} = \frac{9\,(1-v^2)\,a^2}{80\,\pi\,E\,t_m^3}, \tag{3.3}$$

and in collapsed mode, it increases with increasing contact radius.

The instantaneous values of C and C_{Rm}, and hence the transduction force, are determined by the instantaneous rms displacement. The static and instantaneous values are the same for each of these lumped model elements and force.

Since the through variable in the model is chosen as rms velocity, the model inductance, which conserves the energy, is the mass of the membrane [35, 37, 49]:

$$L_{Rm} = \pi\,a^2\,t_m\,\rho. \tag{3.4}$$

The dynamic lumped element model is completed by terminating the acoustic port by appropriate radiation impedance. The radiation impedance Z_{RR} is dependent on the instantaneous contact radius, and consequently on rms displacement.

A large set of static bending calculations is obtained in order to define the lumped parameters' dependence on x_R, t_g/t_{ge} and P_b/P_g. For each bending profile solution, C is calculated first and it is used to find f_R and C_{Rm}.

Static analysis solutions for $\overline{x}(\overline{r})$ are obtained at seven different values of $t_g/t_{ge} = 0.4$, 0.5, 0.6, 0.65, 0.73, 0.82, and 0.9, and interpolation can be done for intermediate values. When t_g/t_{ge} is less than 0.4, the profile is the same as for uniform force distribution. When t_g/t_{ge} is chosen larger than 0.9, the iterations do not converge, hence the model is valid beyond this value.

For each t_g/t_{ge} value, $P_b/P_g = 0$, 0.2, 1, and 2 cases are analyzed, because the intermediate values can be accurately interpolated from the data obtained at those static pressure levels.

For each case, the solutions are obtained at 50 values of (V/V_r) between the normalized snapback voltage (the voltage level at which the membrane exits collapse mode) and a large value, 10. So, a total of 1400 normalized cases are analyzed. With each sweep of V/V_r, keeping t_g/t_{ge} and P_b/P_g fixed, we obtained curves of C, C_{Rm} and b.

3.0.1 Capacitance

The capacitance C for a given deflection profile $\overline{x}(\overline{r})$ is

$$C = C_0 \int_0^1 \frac{2\overline{r}}{1-\overline{x}(\overline{r})}\, d\overline{r}. \tag{3.5}$$

$C_0 = \epsilon_0\, \pi\, a^2/t_{ge}$ is the undeflected membrane capacitance.

In Fig. 3.3, the calculated C/C_0 values are plotted as a function of $\overline{x}_R$ for different values of t_g/t_{ge}. For demonstration purposes, only P_b/P_g=0.2 case is given. When the membrane is uncollapsed, the normalized capacitance is not affected by t_g/t_{ge}. In collapsed mode, the membrane can approach the substrate more for larger values of t_g/t_{ge} (thin insulator), and both the capacitance and the rms displacement can be comparatively large. As t_g/t_{ge} decreases (larger insulator thickness), both the displacement and the capacitance assume smaller values. The dashed line is the plot of uncollapsed mode capacitance calculated

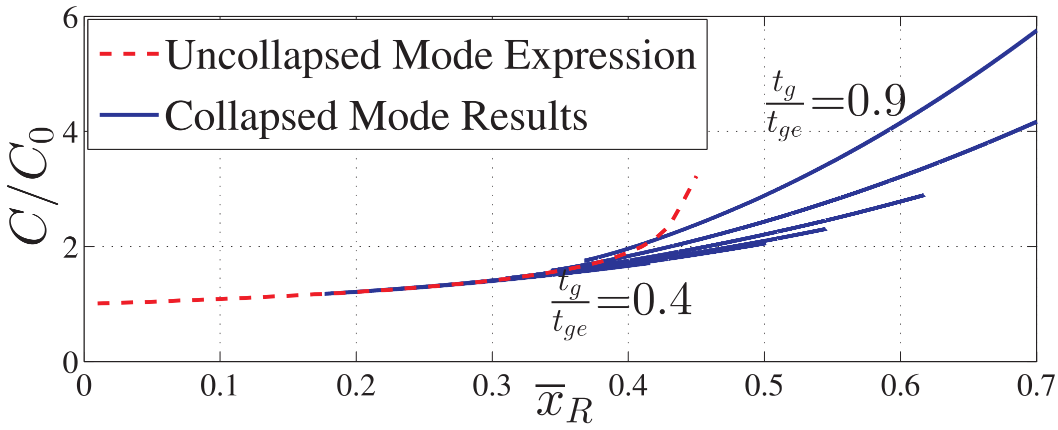

Figure 3.3: Normalized electrical capacitance as a function of normalized rms displacement. $P_b/P_g = 0.2$ and $t_g/t_{ge} = 0.4$, 0.5, 0.6, 0.65, 0.73, 0.82 and 0.9

using the formula of uniform pressure approximation given in Table B.1. The collapsed mode calculations start with the snapback, so the initial points on solid lines correspond to the transition from collapsed mode to uncollapsed mode. However, those points do not coincide with the dashed plot, because of the slight error caused by uniform pressure approximation.

3.0.2 Electrical Force

The electrical force is the energy-conserving force, defined as:

$$f_R = \frac{dE_{el}}{dx_R} = \frac{V^2}{2}\frac{dC}{dx_R} = \frac{V^2}{2\,t_{ge}}\frac{dC}{d\overline{x}_R}. \tag{3.6}$$

$dC/d\overline{x}_R$ term is introduced into the lumped model. With C/C_0 data in hand, $dC/d\overline{x}_R$ is numerically derived for all t_g/t_{ge} and P_b/P_g. The capacitance and the capacitance derivative are defined as separate functions of $\overline{x}_R$ for every P_b/P_g and

t_g/t_{ge} pair.[1]

3.0.3 Compliance

The compliance of the membrane is defined as the ratio of x_R to the rms force on the membrane. In our deflection profile calculations, this force is the sum of the static electrical force F_R and the static uniform force $F_{Rb} = P_b \pi a^2 \sqrt{5}/3$:

$$C_{Rm} = \frac{x_R}{F_R + F_{Rb}}. \tag{3.7}$$

The plot of rms displacement as a function of rms restoring force at different

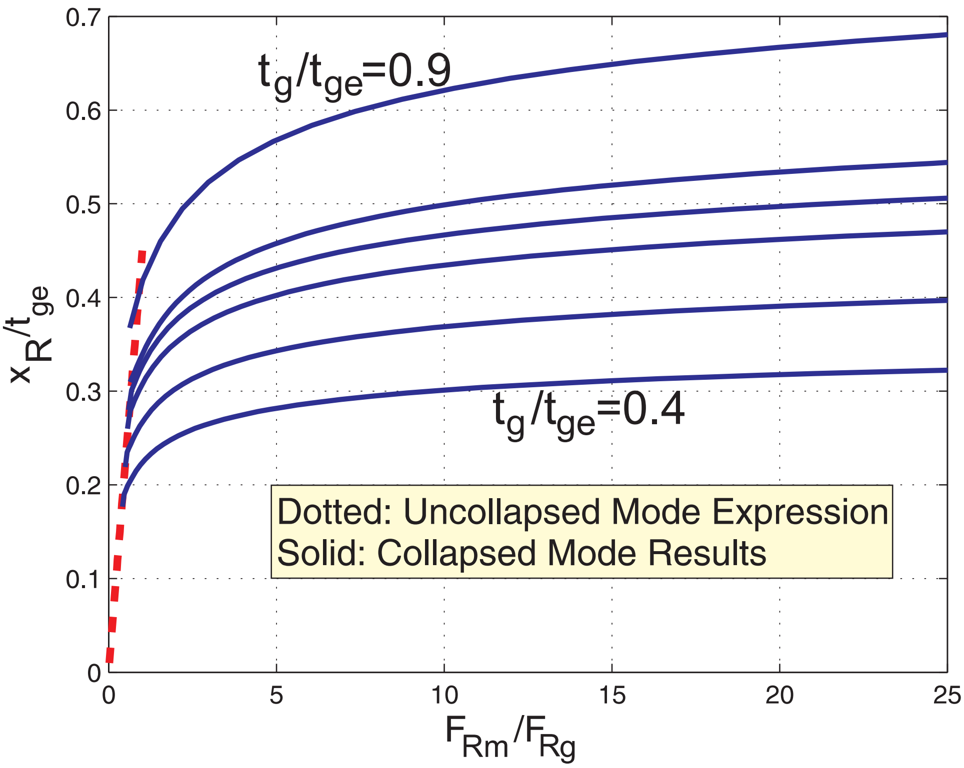

Figure 3.4: Normalized rms displacement as a function of normalized restoring force of the membrane in uncollapsed mode (dotted) and in collapsed mode (solid) for $P_b/P_g = 0.2$ and t_g/t_{ge}=0.4, 0.5, 0.6, 0.65, 0.73, 0.9.

t_g/t_{ge} values is given in Fig.3.4. $\overline{x}_R$ is plotted with respect to F_{Rm}/F_{Rg}, where

[1] Observing that the P_b/P_g dependencies of capacitance and capacitance derivative are weak, it is possible to use the $P_b/P_g = 0.2$ data for all values of static pressure.

$F_{Rm} = F_R + F_{Rb}$, $F_{Rg} = P_g\, \pi\, a^2\, \sqrt{5}/3$ (F_{Rb}/F_{Rg}=0.2 in this case). The uncollapsed mode expression, $F_{Rm}/F_{Rg} = \sqrt{5}\,\overline{x}_R$, is also plotted as the dotted line. In the uncollapsed mode, the membrane behaves like a linear spring. In the collapsed mode, the relation is nonlinear. As the contact radius increases, the membrane gets stiffer, and more force is needed to bend it further.

The normalized compliance C_{Rm}/C_{Rm_0} is plotted with respect to $\overline{x}_R$ in Fig. 3.5 for different t_g/t_{ge} values with P_b/P_g=0. In the stable region of the uncollapsed mode, the membrane has fixed compliance C_{Rm_0}. In the unstable region of the uncollapsed mode, the compliance assumes higher values than C_{Rm_0}. When the membrane gets in contact with the bottom layer (this is also the snapback point), the compliance decreases nonlinearly with increasing displacement. The membrane gets stiffer at larger contact radii. The point of contact is determined by the thickness of insulator. For $t_g/t_{ge} = 0.4$ case, the insulator is so thick that the membrane touches the bottom layer without experiencing instability. On the other hand, for $t_g/t_{ge} = 0.9$, there is a wide region of instability at the end of which the compliance reaches a high value.

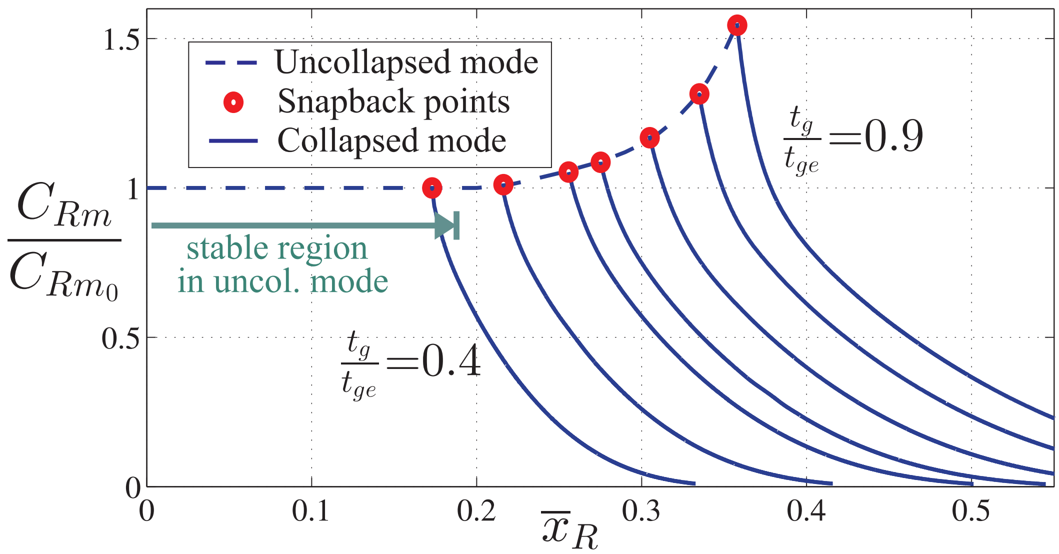

Figure 3.5: Normalized compliance of the membrane as a function of normalized rms displacement. $P_b/P_g = 0$ and $t_g/t_{ge} = 0.4$, 0.5, 0.6, 0.65, 0.73, 0.82 and 0.9

In Fig. 3.6, the normalized compliance is plotted for different levels of ambient pressure P_b/P_g ($t_g/t_{ge} = 0.73$ case is shown). At vacuum, the membrane starts with zero deflection at $V = 0$, while there is an initial deflection for $P_b/P_g = 0.2$, 1 or 2. For $P_b/P_g = 1$ or 2, the ambient pressure is so large that the membrane touches bottom even at $V = 0$; hence it is always in collapse mode. For P_b/P_g = 2, the initial deflection is larger, and the initial compliance is correspondingly smaller. In the collapsed mode, the compliance at the same displacement turns out to be larger for higher ambient pressure.

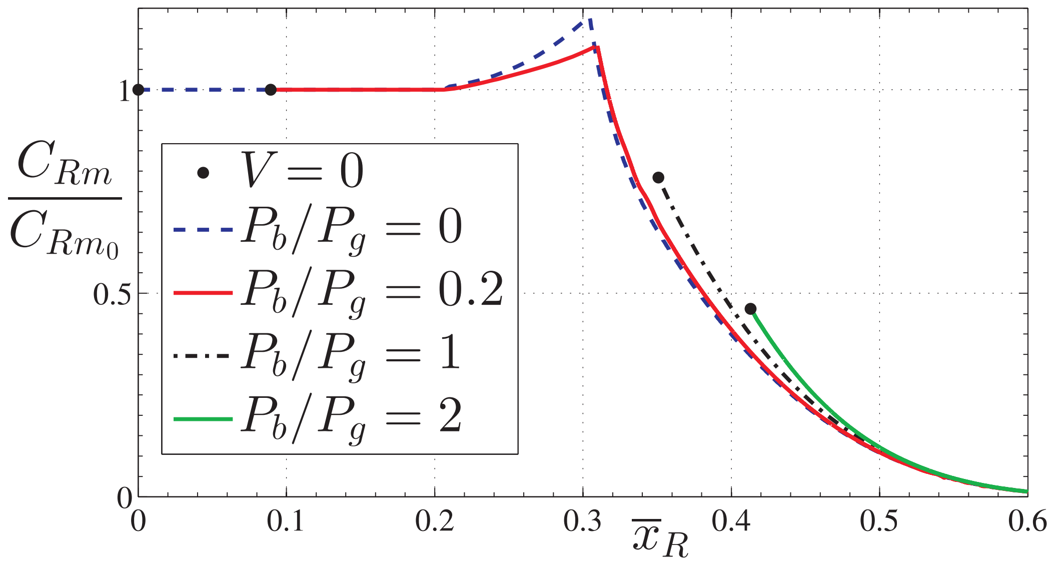

Figure 3.6: Normalized compliance of the membrane as a function of normalized rms displacement for $t_g/t_{ge} = 0.73$ and $P_b/P_g = 0$, 0.2, 1 and 2. Black dots show the initial displacements at $V = 0$.

3.0.4 Contact Radius

Fig. 3.7 shows the normalized contact radius, $\overline{b}$, as a function of $\overline{x}_R$ for two values of P_b/P_g and for different values of t_g/t_{ge}. For $P_b/P_g = 1$, ambient pressure is strong enough to make the membrane touch the bottom layer even at zero voltage. So the $P_b/P_g = 1$ plots start at nonzero $\overline{b}$ values.

We observe significant difference between the solid and dashed plots of t_g/t_{ge}=0.9 case. Close to snapback, they assume very different $\overline{x}_R$ values at the same contact radius. This is because the bending profiles of uniform pressure-deflected and electrical force-deflected membranes are considerably different in collapsed mode.

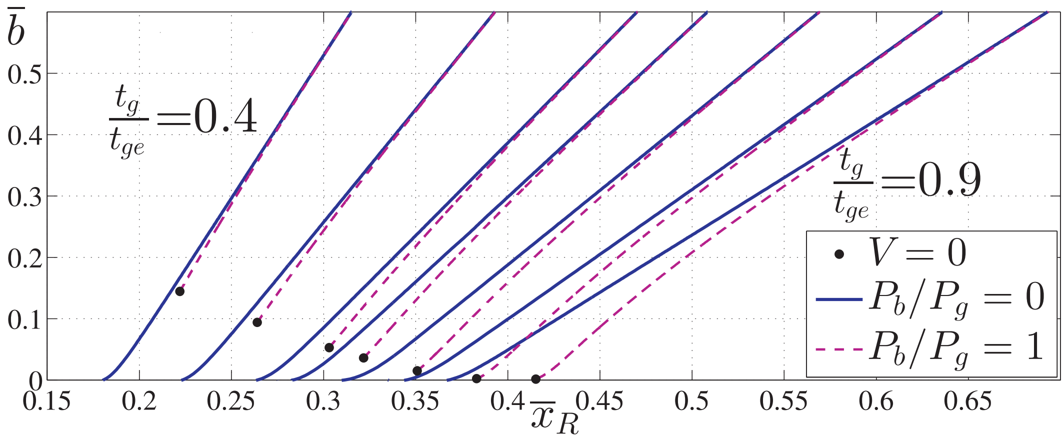

Figure 3.7: Normalized contact radius as a function of normalized rms displacement for P_b/P_g = 0, 1, and t_g/t_{ge} = 0.4, 0.5, 0.6, 0.65, 0.73, 0.82, and 0.9. $\overline{b}$=0 corresponds to snapback point.

3.0.5 Discussions

In order to adapt all the calculations to the lumped model, polynomials are fitted to the numerical results of $C(\overline{x}_R)/C_0$, $dC(\overline{x}_R)/d\overline{x}_R$, $C_{Rm}(\overline{x}_R)/C_{Rm_0}$, and $\overline{b}(\overline{x}_R)$. As we can record finite number of data, the results at discrete values of P_b/P_g and t_g/t_{ge} are included in the model. The results at the remaining values are obtained using linear interpolation. The polynomial coefficients of a sample case, $P_b/P_g = 0.2$ and $t_g/t_{ge} = 0.73$, are given in the Appendix.

Fig.3.8 shows the reliability of linear interpolation for the restoring force. t_g/t_{ge}=0.5 and t_g/t_{ge}=0.65 results are linearly interpolated to reach t_g/t_{ge}=0.6 result, and the approximation is consistent with calculated results. Similarly, interpolation can be used for capacitance and compliance.

While obtaining datasets for the membrane compliance, we observed that the normalized compliance can be approximately expressed as a unique function of x_R/t_g for a given P_b/P_g. It means, two CMUTs with the same membrane

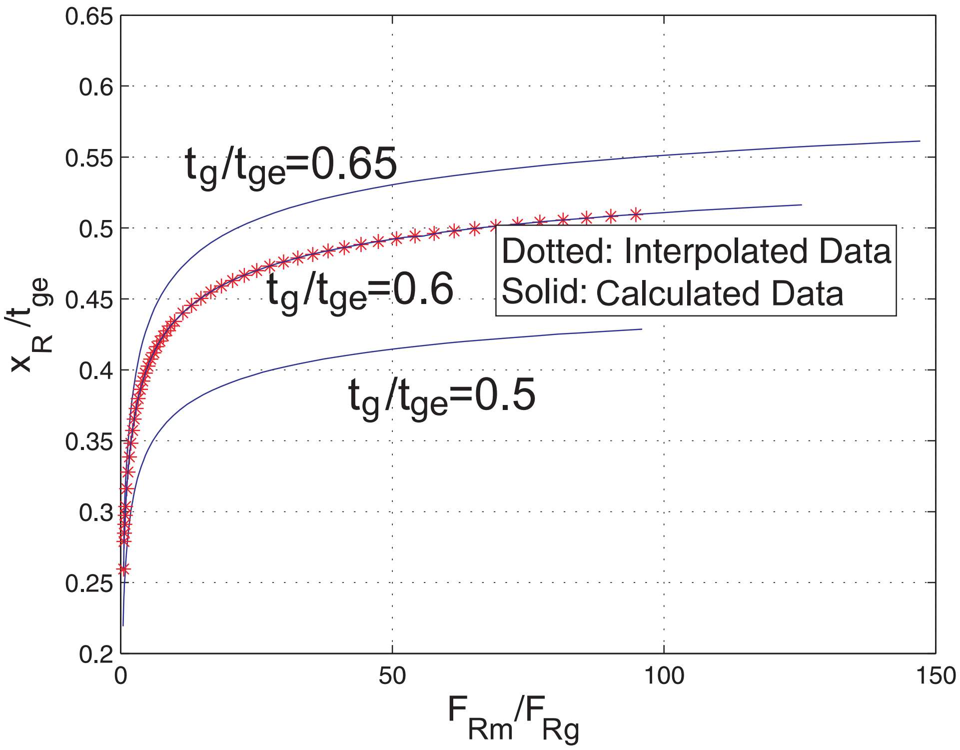

Figure 3.8: Interpolated value of $\overline{x}_R(F_{Rm}/F_{Rg})$ compared to the calculated value. t_g/t_{ge}=0.6 data is obtained from t_g/t_{ge}=0.5 and t_g/t_{ge}=0.65 data.

dimensions will have approximately the same compliance for the same x_R/t_g values. In Fig.3.9, CMUT 2 has the same membrane dimensions with CMUT 1, where its gap height is twice the gap height of CMUT 1, $t_{g_2} = 2\, t_{g_1}$. In this case, $C_{Rm_2}(x_R) \simeq C_{Rm_1}(x_R/2)$.

Using this approximation, a single compliance function can be used to derive the compliance of all t_g/t_{ge} values, for a fixed P_b/P_g value. In Fig.3.10, using t_g/t_{ge}=0.65 data, the compliance functions for all the other t_g/t_{ge} values are obtained through the formula

$$C_{Rm_n}(x_R) = C_{Rm_{0.65}}\left(x_R \frac{0.65}{n}\right), \qquad (3.8)$$

where $n = t_g/t_{ge}$.

Dotted lines show the curves obtained using t_g/t_{ge}=0.65 data, and the solid

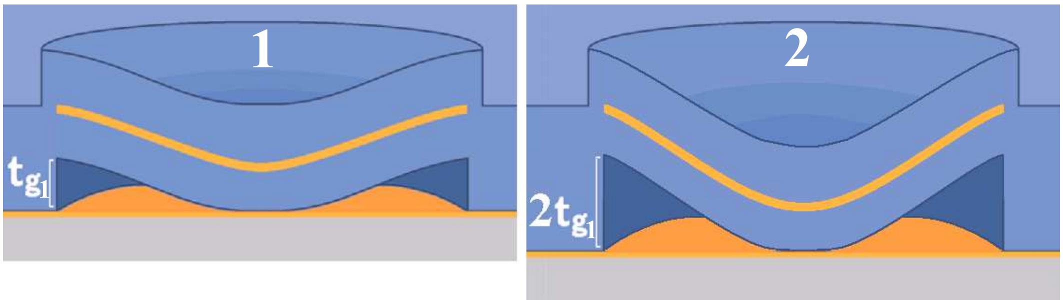

Figure 3.9: Two CMUTs with the same membrane dimensions, different air gap height.

lines show the numerically calculated compliance plots for each of the t_g/t_{ge} values. There is good agreement up to t_g/t_{ge}=0.82.

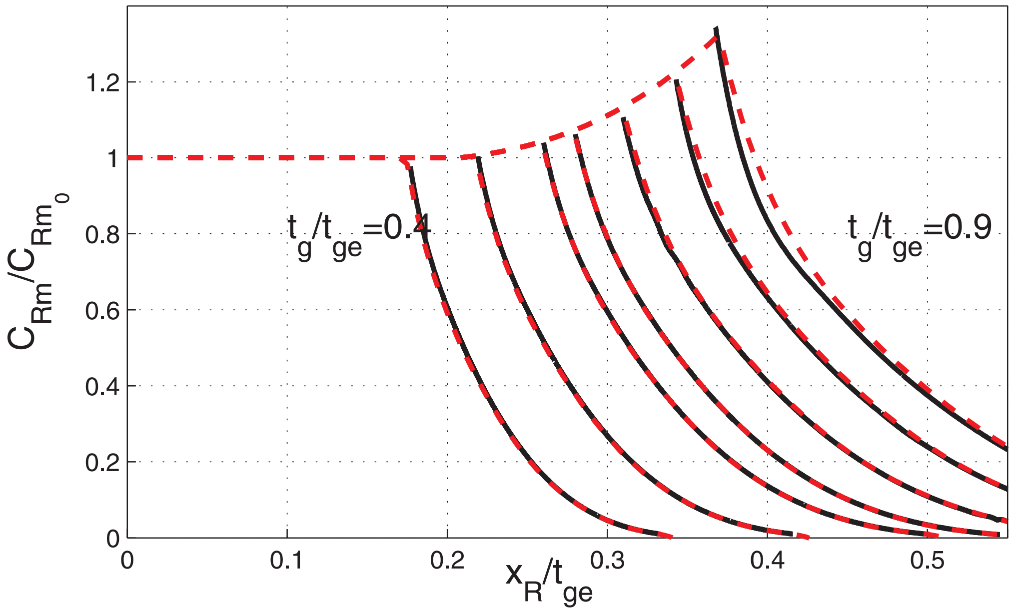

Figure 3.10: Normalized compliance of the membrane obtained using x_R/t_g normalization. t_g/t_{ge} = 0.4, 0.5, 0.6, 0.65, 0.73, 0.82 and 0.9 plots are all obtained through t_g/t_{ge}=0.65 compliance(dotted). The calculations for each t_g/t_{ge} are also given with solid lines. $P_b/P_g = 0.2$

Chapter 4

Collapsed Mode Radiation Impedance

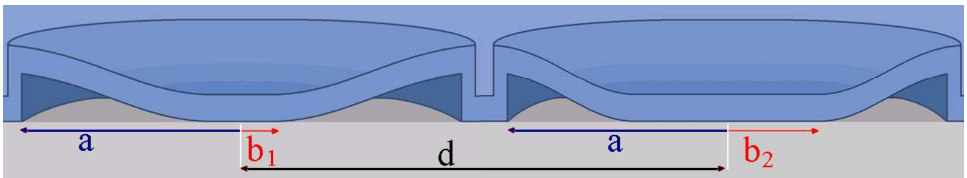

Figure 4.1: Neighboring CMUTs.

In the uncollapsed mode, the self radiation impedance of a cell is dependent on the operation frequency and membrane radius, and for the mutual radiation impedance between two cells, the cell-to-cell distance is another factor. In the collapsed mode, self and mutual radiation impedances also depend on the contact radii of the CMUT and its neighbor (see Fig.4.1). The self and mutual radiation impedances in collapsed mode operation should be introduced as a function of contact radii.

The interaction between the CMUT membrane and the radiation medium is determined by the velocity profile of the membrane. In uncollapsed mode, the entire membrane surface is active, whereas the periphery beyond the contact point is the active region in collapsed mode as in Fig.4.2. The radiation impedance of

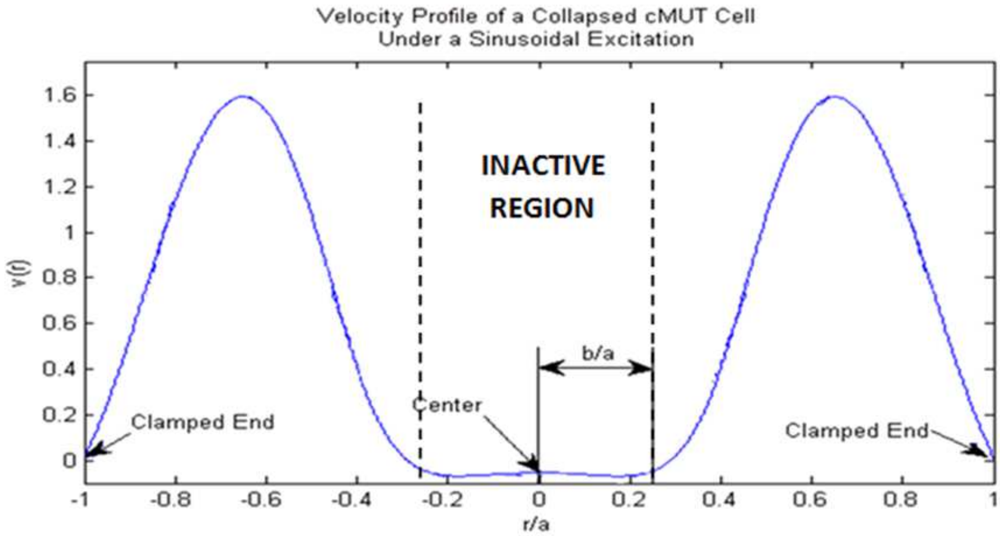

Figure 4.2: The velocity profile of the collapsed CMUT membrane.

this type of membrane is calculated by Alper Ozgurluk [51] and given as:

$$Z_{RR} = \pi\, a^2\, \rho_0\, c_0\, \{R_1(ka) + j\, X_1(ka)\}. \tag{4.1}$$

The real and imaginary parts of normalized self radiation impedance are plotted in Fig. 4.3 as a function of ka (k is the wavenumber) for different values of $\overline{b}$. Here, the $\overline{b} = 0$ curve is the same as the uncollapsed mode self radiation impedance. For ka<0.5, there is slight difference in impedance at different contact radii. As ka increases, the impedance becomes strongly dependent on the contact radius. For ka>16 ($radius/wavelength \simeq 2.5$), $Z(ka) \simeq 1$ for all cases.

For the mutual radiation impedance between two CMUTs, $\overline{b}_1$, $\overline{b}_2$ (the contact radii of the CMUTs), and d (center-to-center distance) are additional factors. In Fig. 4.4, the real and imaginary parts of the normalized mutual radiation impedance are plotted as a function of kd, for $ka = 1$, $\overline{b}_1 = 0.3$, and $\overline{b}_2$ =0, 0.2, 0.4 and 0.6. In this plot, the mutual radiation impedance seems to weakly depend on the contact radius. However, this situation changes with increasing ka. In Fig. 4.5, impedance is plotted as a function of kd, at $ka = 3$. In this figure, we observe strong dependence on the contact radius.

In Fig. 4.6, kd is fixed to 6, and the normalized mutual radiation impedance

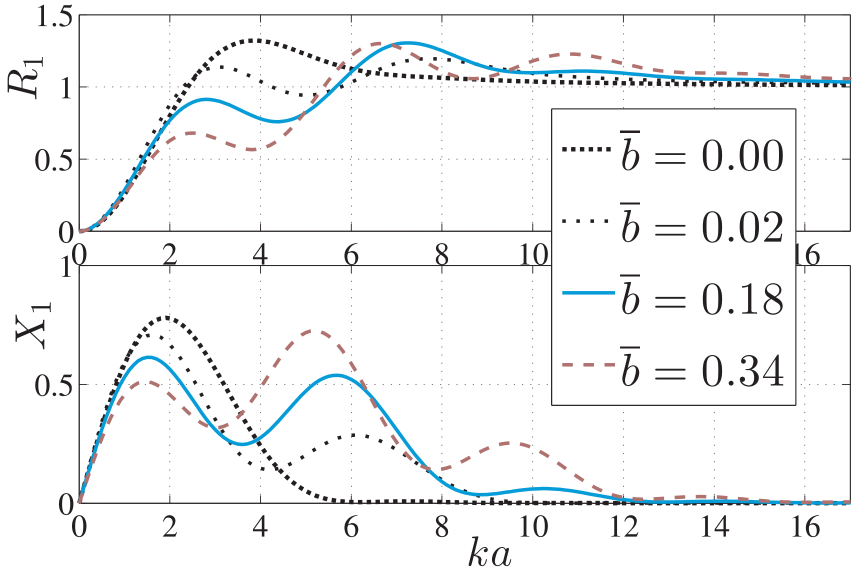

Figure 4.3: The real (upper figure) and imaginary (lower figure) parts of self radiation impedance of a CMUT in collapsed mode as a function of ka for various normalized contact radii, $\overline{b}$.

is plotted as a function of ka. A similar plot is obtained for $kd = 30$ in Fig. 4.7.

For fixed a and d, the change in mutual radiation impedance with changing frequency is shown in Fig. 4.8 where $d = 2.1\,a$, and in Fig. 4.9 where $d = 5\,a$.

All the figures show that the mutual radiation impedance strongly depends on the contact radii of the cells, and the dependence is not linear or can be handled through simple expressions. So the impedance should be introduced to the model as a function of two contact radii. The only exception is small signal operation, in which all the CMUTs in an array have almost the same contact radius at a time point. For such simulations, the impedance data can be introduced as a function of single contact radius for both cells.

For the equivalent circuit model, we record the self and mutual radiation impedance data at discrete values of all parameters, and use the data as a lookup table. For the self radiation impedance, we use 9 values of contact radii, up to $\overline{b} = 0.6$. The required Z_{RR} value is interpolated dynamically in the contact radius space. Similarly, the mutual radiation impedance data is also recorded at discrete

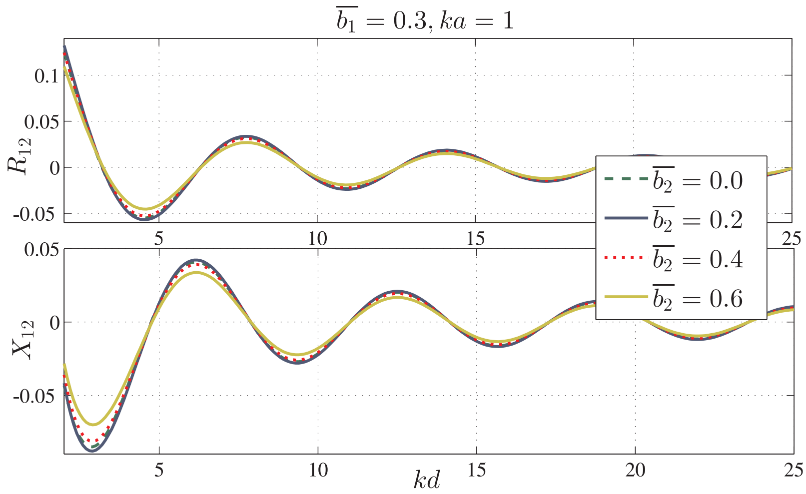

Figure 4.4: The real (upper figure) and imaginary (lower figure) parts of mutual radiation impedance of a CMUT in collapsed mode as a function of kd for $\overline{b}_1$=0.3 and $\overline{b}_2$=0, 0.2, 0.4, 0.6. $ka = 1$.

values of contact radius pairs, up to $\overline{b}_1 = 0.6$ and $\overline{b}_2 = 0.6$. The use of Z_{RR} data in ADS[3], and construction of an array model is described in the Appendix.

[3]Advanced Design System from Agilent Technologies

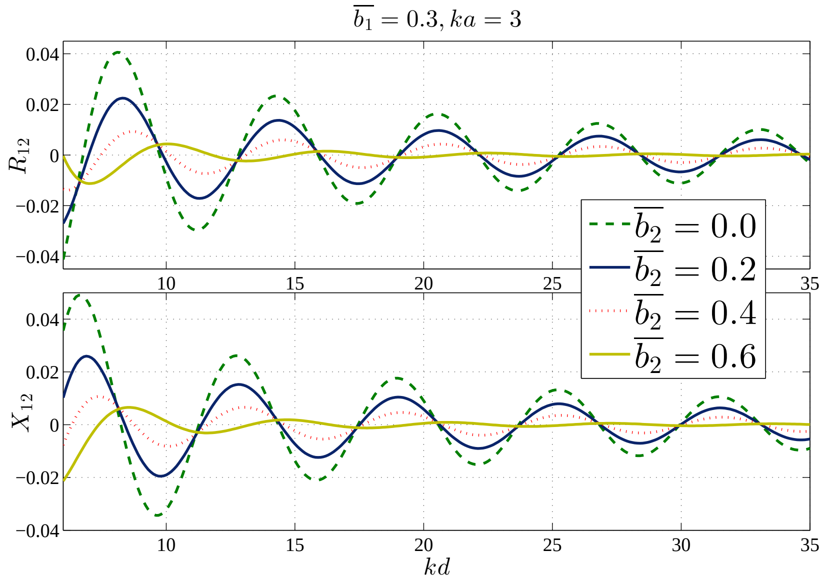

Figure 4.5: The mutual radiation impedance of a CMUT in collapsed mode as a function of kd for $\overline{b}_1$=0.2 and $\overline{b}_2$=0, 0.2, 0.4, 0.6. $ka = 3$.

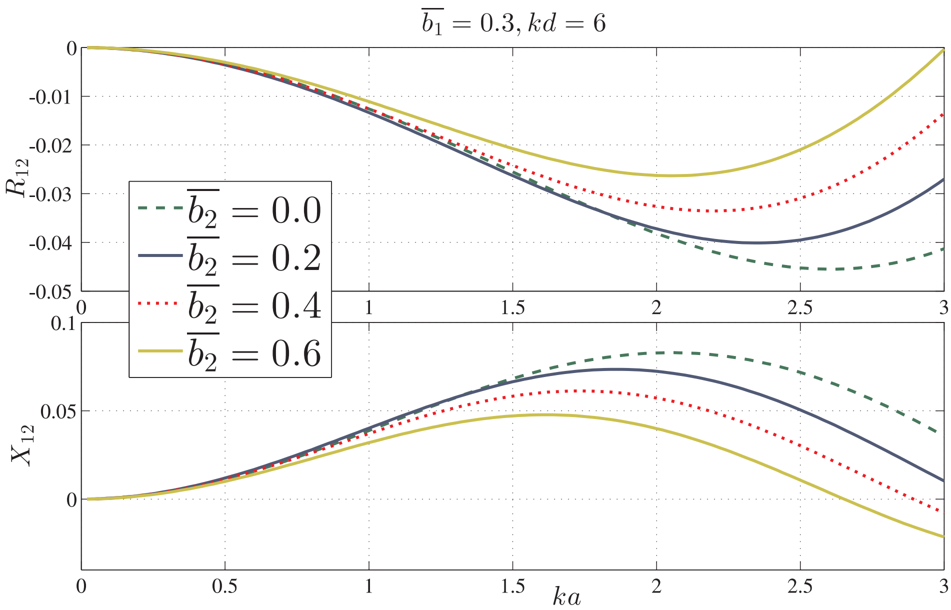

Figure 4.6: The mutual radiation impedance of a CMUT in collapsed mode as a function of ka for $\overline{b}_1$=0.2 and $\overline{b}_2$=0, 0.2, 0.4, 0.6. $kd = 6$.

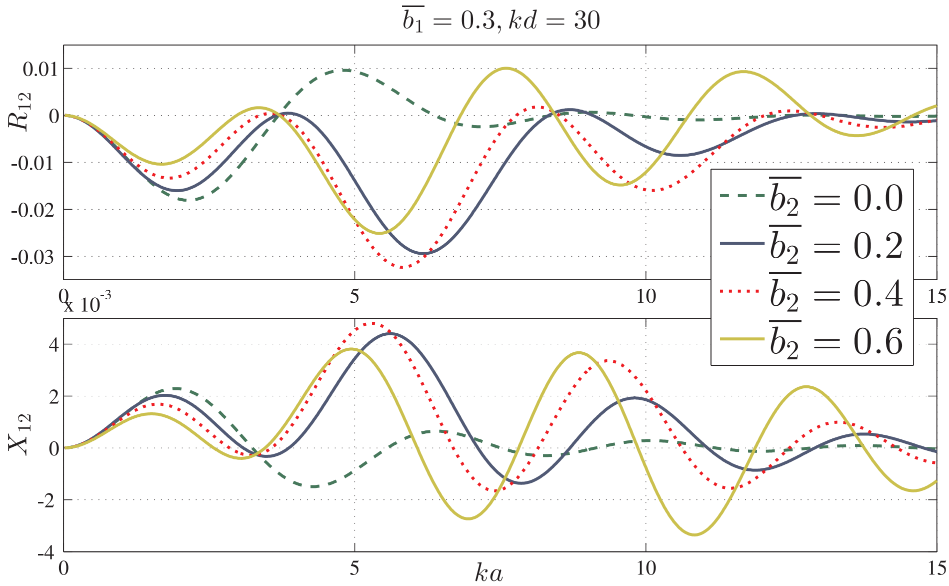

Figure 4.7: The mutual radiation impedance of a CMUT in collapsed mode as a function of ka for $\overline{b}_1$=0.2 and $\overline{b}_2$=0, 0.2, 0.4, 0.6. $kd = 30$.

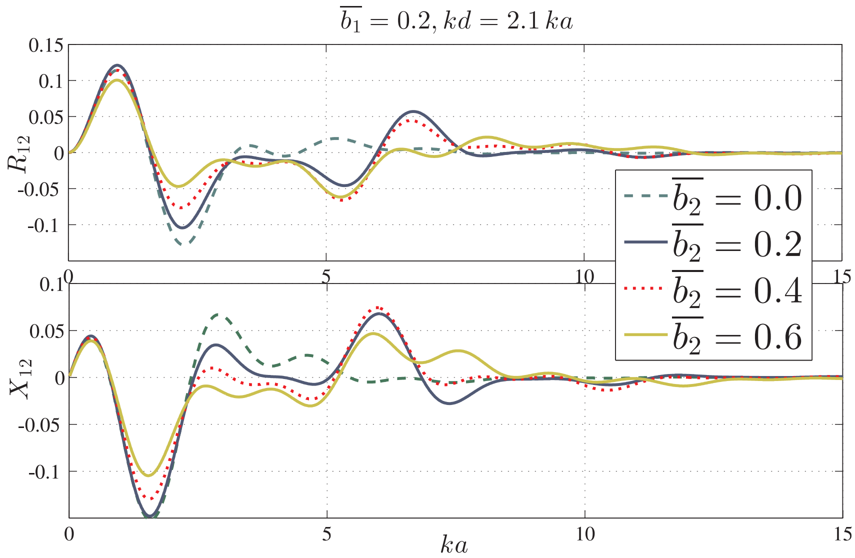

Figure 4.8: The mutual radiation impedance of a CMUT in collapsed mode as a function of ka for $\overline{b}_1$=0.2 and $\overline{b}_2$=0, 0.2, 0.4, 0.6. $kd = 2.1\,ka$.

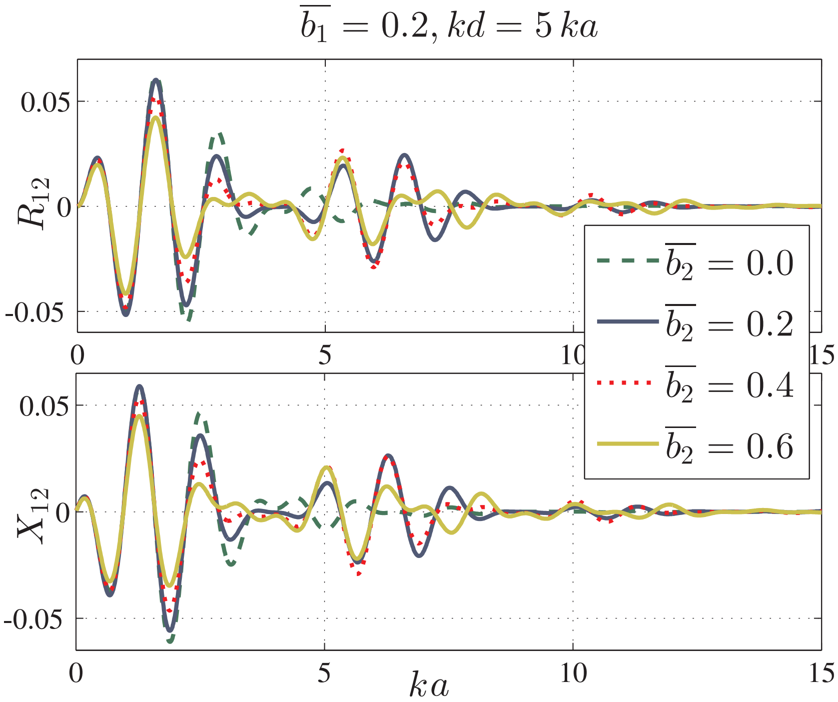

Figure 4.9: The mutual radiation impedance of a CMUT in collapsed mode as a function of ka for $\bar{b}_1$=0.2 and $\bar{b}_2$=0, 0.2, 0.4, 0.6. $kd = 5\,ka$.

Chapter 5

Simulations with Equivalent Circuit Model of Uncollapsed and Collapsed Mode CMUT

The equivalent electrical circuit is simulated with ADS[3], a time-domain circuit simulator capable of handling frequency domain input data. Parameter values used in the following simulations are given in Table 5.1.

Table 5.1: Parameters of CMUT cell used in simulations

E	υ	ϵ_r	ρ
110 GPa	0.27	5.4	3.1 g/cm^3
a	t_m	t_i	t_g
30 μm	1.2 μm	0.4 μm	0.2 μm

The transient response of a CMUT under large sinusoidal excitation is shown in Fig. 5.1. The equivalent circuit simulations are given together with the FEA [4] simulations. The CMUT is in water, and all the parameters are as given in Table 5.1, except $t_m = 1.4\mu$m and $t_i = 0.2\mu$m. The resonance frequency of the

[3]Advanced Design System from Agilent Technologies

[4]FEA simulations are carried out in ANSYS 13.0. A 2-D axisymmetric model of a single CMUT is created as in [51].

membrane is 4.57MHz in the uncollapsed mode. The applied DC voltage is larger than the collapse voltage (37V). On top of the DC voltage, a 5MHz AC signal of 30V amplitude is applied. The simulations show that the CMUT operates at a lower frequency, 2.5MHz. Only at one of each two cycles, the membrane experiences collapse mode. In every other cycle, the rms displacement becomes negative, the instantaneous gap height becomes very large, and the electrical force is very small. In those cycles, the increase in the voltage and the electrical force cannot pull the membrane back. So, the response is observed at half of the drive frequency. The equivalent circuit model is successful in predicting this response.

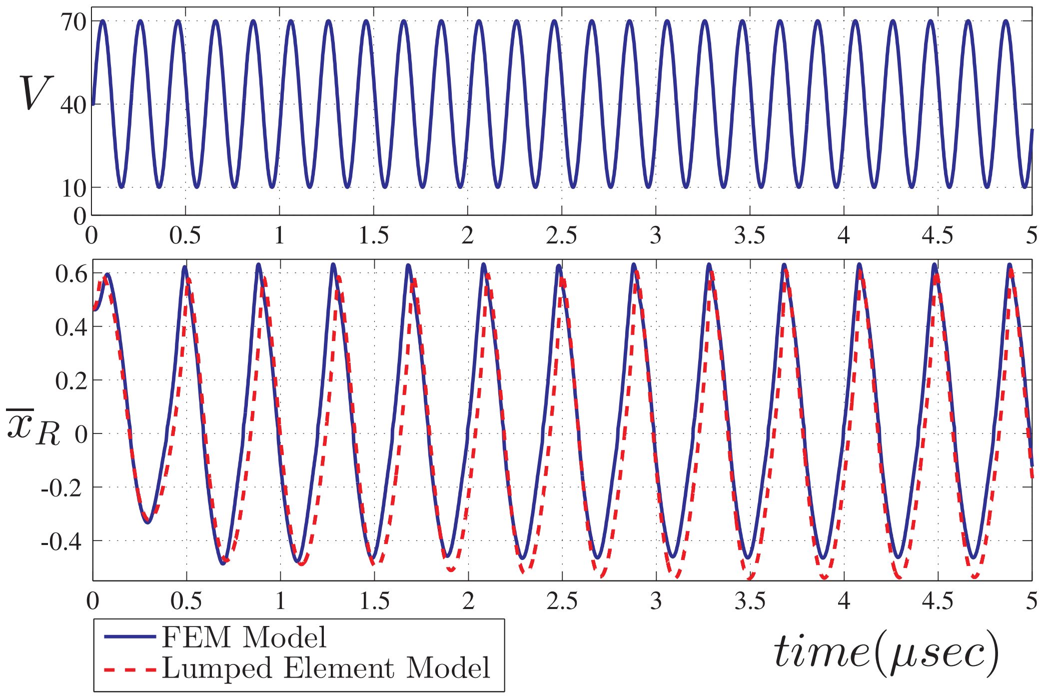

Figure 5.1: The transient response of single CMUT under large sinusoidal excitation in water, predicted by lumped element and FEM simulations (P_b=0).

In Fig. 5.2, the positive and negative ramp signal response (in water) is given. The medium pressure is assumed to be zero. FEA simulations are added for comparison. The collapse timing is the same for both simulations, while there is a slight difference in snapback timing. According to the model, the snapback occurs at 31.5V. FEM simulation predicts the snapback at 32V. Since a single CMUT is considered, the radiation resistance is rather low and the membrane is lightly loaded. At the frequency of oscillation in uncollapsed mode, ka is small at about 0.2 and the approximate value of the radiation impedance Z_{RR} is 42.4 (1 + j10) μN-s/m. The quality factor of the radiation impedance is already about 10. The mass of the membrane increases this further. So, the bandwidth is quite small, and slowly decaying oscillations are observed after the sudden pull and release of the membrane.

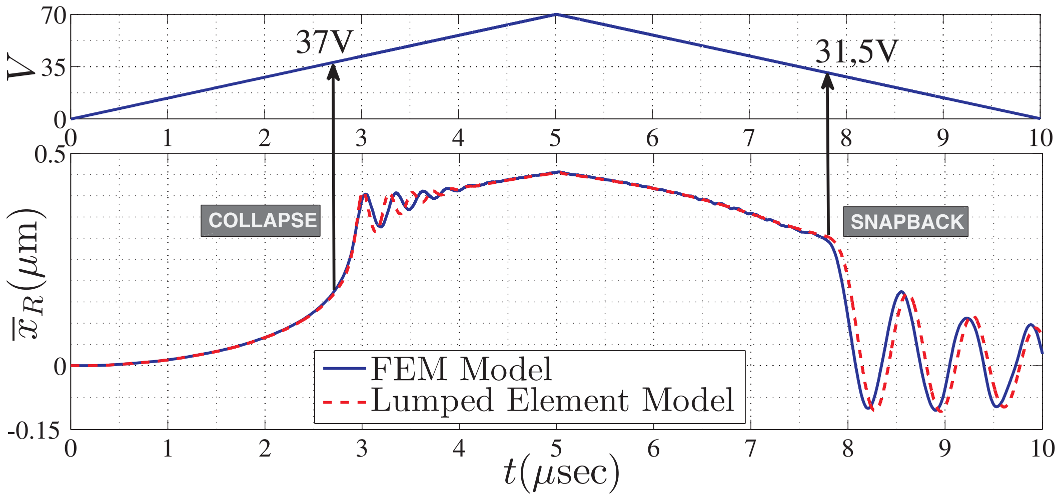

Figure 5.2: The collapse and snapback behavior of the CMUT of Table 5.1 in water, predicted by lumped element and FEM simulations (P_b=0).

In the collapsed mode, the resonance frequency is not fixed, since the membrane compliance decreases with increasing deflection. Fig. 5.3 depicts the resonance frequency, at which the maximum amount of real power is delivered to the medium, as a function of the DC bias voltage. Here, the CMUT of Table 5.1 is driven in water with an AC signal of 1V peak voltage. The uncollapsed region is also plotted. As the bias voltage is increased toward the collapse voltage, the resonance frequency decreases slightly. But as soon as the membrane collapses, the membrane stiffness, and the resonance frequency increases. As the collapse radius gets larger, the membrane becomes even stiffer and the resonance frequency increases monotonically. The dashed line in the same figure shows the amplitude of the pressure on the medium radiation resistance at the corresponding resonance frequencies. Notice that at a bias voltage of 100V, the CMUT generates a pressure of more than 55kPa/V.

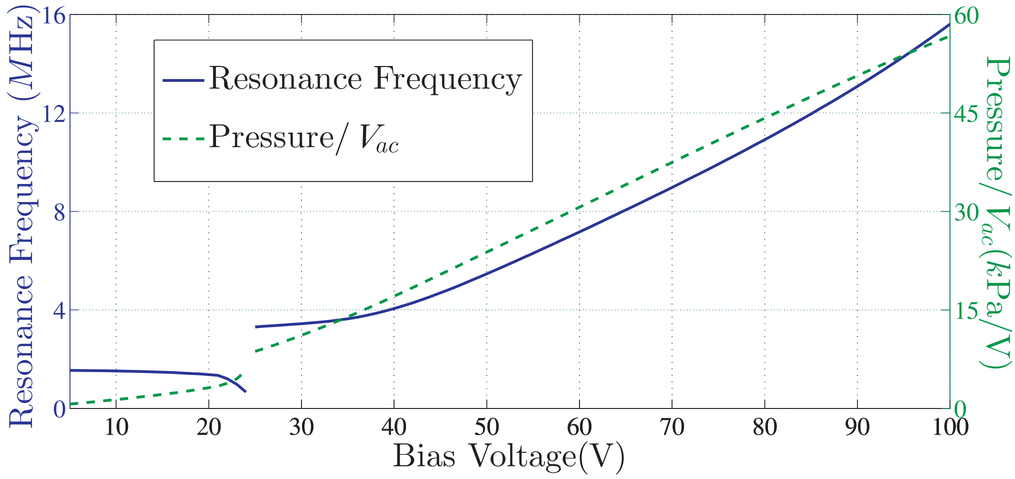

Figure 5.3: The resonance frequency of a single CMUT (Table 5.1, in water, P_b = 1atm) and the pressure on the real part of the self radiation impedance at the resonance frequency as a function of bias voltage, as predicted by the lumped element model.

As an application of the model, a CMUT cell in water at ambient pressure is driven with a 50V pulse of 10 nsec rise and fall times. The maximum instantaneous pressure across the membrane surface is plotted as a function of membrane radius a. The other dimensions of the CMUT cell are kept fixed at $t_m = 1\mu$m, $t_i = 0.1\mu$m, and $t_g = 0.1\mu$m. The solid curve of Fig. 5.4 gives the maximum instantaneous pressure obtained at the rising edge of the voltage pulse (collapsing), and the dashed line gives the maximum pressure at the falling edge (at snap-back). As the radius of the membrane is increased, the collapse voltage reduces. For $a < 11.4\mu$m, the collapse voltage is higher than 50V; hence collapse never occurs. The resulting pressure is relatively low. When $a > 11.4\mu$m, collapse occurs on the rising edge. The pressure maximum increases almost 10 times. As a is increased further, the membrane is driven more and more in the deep-collapse mode. The pressure maximum at the rising edge increases monotonically as the cell radius is increased. This prediction is consistent with the measurement results of CMUTs in deep-collapse mode [48]. On the other hand, the pressure maximum at the falling edge seems to be saturated around a constant value.

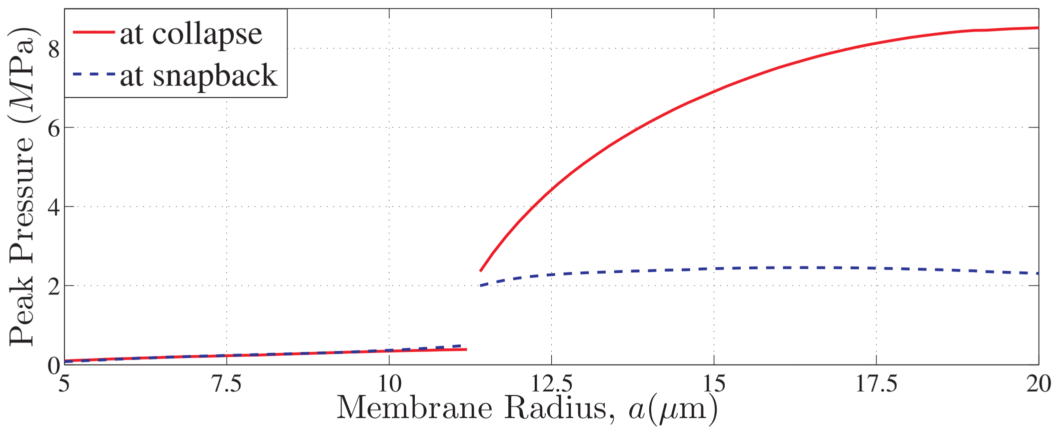

Figure 5.4: The maximum instantaneous pressure at the membrane surface as a function of radius, at the rising (collapsing) and falling (snapback) edges of a $50V$ pulse at ambient pressure in water.

Chapter 6

Conclusions

In this work, an equivalent circuit model for the collapsed mode operation of CMUT is obtained. The static deflection profile of a circular CMUT in collapsed mode is numerically calculated by introducing the radial distance dependent electrical force into Timoshenko's equation. Using this force profile, the deflection profile and the snapback point are calculated precisely. The static deflection profile solutions are used to determine the electrical capacitance, the electrical force, the mechanical compliance of the membrane for various CMUTs of different dimensions and physical parameters, under different pressure and voltage levels. The calculations are carried out in a normalized basis, so that any CMUT's model can be constituted through simple arithmetical calculations using this basis.

There are three main parameters that determine the deflection profile of collapsed mode CMUT; the air gap height normalized to the effective gap height (t_g/t_{ge}), the uniform pressure on the membrane normalized to a reference pressure (P_b/P_g), and the applied voltage normalized to the collapse voltage (V/V_r). 1400 static deflection calculations are carried out for t_g/t_{ge} = 0.4, 0.5, 0.6, 0.65, 0.73, 0.82, and 0.9; P_b/P_g=0, 0.2, 1, and 2; (V/V_r) between the normalized snapback voltage (the voltage level at which the membrane exits collapse mode) and a large value, 10. The model is valid in the range of those values. Interpolation can be done for intermediate values. The results are used to obtain the curves of C, C_{Rm} and b. The model is merged with the uncollapsed mode model to obtain a single model for simulating the whole operation of CMUT.

In the collapsed mode, the self and mutual radiation impedances depend on the contact radius. The self and mutual radiation impedances are introduced to the model as a set of lookup tables, for discrete values of $\bar{b}<0.6$, and an instantaneous interpolation is used.

As the circuit elements are expressed through polynomials that are fitted to numerical calculations, inaccuracy may result from slight differences in calculations and the fitted polynomials. The interpolation between discrete data is another source of inaccuracy. There is a compromise between computation cost and accuracy; considering the needs, the degrees of the fitted polynomials and the number of discrete data can be increased for better accuracy.

Transient simulations of single CMUT cell are closely consistent with FEA results. Collapse, snapback, and the decaying oscillations following sudden collapse and release of the membrane are successfully predicted by the model.

Simulations with the model show that high transmit pressures can be achieved by operating in the collapse mode. The reason is the reduced gap height at the contact region, where larger electrical force is obtained with the same voltage. Also we observed that the membrane stiffness increases nonlinearly with increasing contact radius, and the membrane can store larger energy at larger deflection, and high force is available when it is released.

We can predict any large or small-signal operation of a single CMUT in the order of minutes. The same transient simulation takes ~100 times longer with FEA. The model can simulate arrays of collapsed mode CMUTs, which are impossible to simulate with FEA due to computation cost. An array of 10x10 CMUTs can be simulated in ~30 sec/frequency speed in AC analysis. Study on array modeling still continues with parameter optimizations and testing, and no simulations are given in this thesis.

Even in arrays working in uncollapsed mode, some CMUTs may experience collapse mode due to crosstalk. With our model, arrays containing CMUTs operating both in collapsed and uncollapsed modes can be simulated. The model is expected to accelerate the studies on the collapsed mode, and improve the performance of CMUT operation by offering fast simulation opportunity. The effect of any parameter on the performance can be determined very quickly, and the model can be used to optimize CMUT geometries or find the optimum driving voltage waveform for the highest transmit power, and the best receive sensitivity.

Appendix A

Calculation of Deflection Profile

The routine for calculating the deflection profile of the collapsed CMUT membrane is described in Chapter 2. The calculations are carried out in MATLAB using the following code, described within the command lines:

```
%Numerical calculation of static deflection profile of collapsed ...
    mode CMUT

%OUTPUT
%Xrms: rms membrane displacement normalized to effective gap height
%C: Electrical capacitance normalized to undeflected memb. ...
    capacitance
%bpre: Contact radius normalized to membrane radius

%INPUT
%Pn: Uniformly distributed pressure on the membrane normalized ...
    to Pg
%Vn: Applied voltage normalized to collapse voltage
%tn: Air gap height normalized to effective gap height
function [Xrms,C,bpre]=collapsed(Pn,Vn,tn)

eps=8.854e-12;
syms q real
```

```
Fpoly=64*(Pn+2/9*Vn^2/(1-tn)^2*(1-q)*1.5); %initial guess of ...
    force density

db=1;
bpre=0;

%THE ITERATIONS CONTINUE UNTIL THE NORMALIZED CONTACT RADIUS ...
    CONVERGES
while abs(db)>0.0001
%db: difference between the contact radius results of adjacent ...
    iterations
syms b q real %b: contact radius normalized to membrane radius
              %q: radial distance normalized to membrane radius
syms C1 C2 C3 C4 real

%%%%%%%%%%%%%%%%%%%%%%%%%%%%%%%%%%%%%%%%%%%%%%%%%%%%%%%%%%%%%%%%%%%%
%DEFINE DISPLACEMENT FUNCTION AS GIVEN IN Eq.2.7%%%%%%%%%%%%%
%Y: Normalized displacement as a function of normalized radial ...
    distance
%dY: First radial derivative of displacement function
%ddY: Second radial derivative of displacement function
Y=int((int((int((int(Fpoly*q,q,b,q)+C1)/q,q)+C2)*q,q)+C3)/q,q)+C4;
dY=diff(Y,q);
ddY=diff(dY,q);
%PRODUCE 4 EQUATIONS BY APPLYING THE FIRST 4 BOUNDARY CONDITIONS ...
    OF Eq.2.10
X1=vpa(subs(Y,q,1));
X2=vpa(subs(Y,q,b)-tn);
X3=vpa(subs(dY,q,1));
X4=vpa(subs(dY,q,b));
%SOLVE FOR C1, C2, C3, C4
[G1,G2,G3,G4]=solve(X1,X2,X3,X4,'C1,C2,C3,C4');
%SUBSTITUTE C1,C2,C3,C4, AND EXPRESS Y AND ddY IN TERMS OF q AND b.
C1=G1;
C2=G2;
C3=G3;
C4=G4;
Y=vpa(subs(Y));
ddY=vpa(subs(ddY));
```

```
%DEFINE THE ELECTRICAL FORCE DENSITY DISTRIBUTION, USING Y FUNCTION
F=vpa(64*(Pn+2/9*Vn^2/(1-Y)^2));

%FIND b BY APPLYING LAST BOUNDARY CONDITION OF Eq.2.10
%b can be found by finding the ddY function's zero-intersecting ...
    point
ddY=vpa(subs(ddY,q,b));
b=[1e-3:1e-3:1-1e-3];
der=subs(ddY);
n=interp1(der,b,0);
b=n;
%UPDATE "while" CONDITION AND SET bpre TO OBTAINED b
db=b-bpre;
bpre=b;

%IN Y AND F FUNCTIONS, SUBSTITUTE b WITH THE OBTAINED VALUE
syms q real
Y=subs(Y); % Y(q)
q=[b:(1-b)/1000:1];
yy=subs(Y);
Fq=vpa(subs(F));

%FIT THE ELECTRICAL FORCE DENSITY TO A POLYNOMIAL OF DEGREE 14
syms Fpoly real
PP=polyfit(q,Fq,14);
syms b q qq real
%A spatial adjustment is applied below, in order to prevent very ...
    high forces in the next iteration
qq=q-(b-bpre);
Fpoly=poly2sym(PP,qq);

end

%CALCULATE THE RMS VALUE OF NORMALIZED DISPLACEMENT
Xrms=sqrt(int(2*q*Y^2,q,bpre,1)+bpre^2*tn^2)
%CALCULATE THE NORMALIZED ELECTRICAL CAPACITANCE
q=[bpre:(1-bpre)/1000:1];
dC=2*(1-bpre)/1000.*q./(1-yy);
C=(bpre^2/(1-tn)+sum(dC))
```

Appendix B

Model Parameters

Table B.1 lists all the uncollapsed and collapsed mode expressions for lumped parameters, and the mode transition conditions. For the uncollapsed mode, we have nonlinear equations [35]. For the collapsed mode, we have polynomials for $t_g/t_{ge} = 0.4$, 0.5, 0.6, 0.65, 0.73, 0.82, and 0.9; and $P_b/P_g = 0$, 0.2, 1, and 2.

Continuous transition between collapsed and uncollapsed regions is insured by defining the transition points exactly at the intersections of uncollapsed and collapsed mode expressions.

As an example to the coefficients of the polynomials and the transition points, the $t_g/t_{ge} = 0.73$, $P_b/P_g = 0.2$ case is given in Table B.2. Simulations at intermediate t_g/t_{ge} and P_b/P_g values can be performed using interpolation. For $t_g/t_{ge} = 0.58$ and $P_b/P_g = 0.4$, the instantaneous capacitance and compliance should be calculated as

$$C\big|_{t_g/t_{ge}=0.58} = 0.2\, C\Big|_{t_g/t_{ge}=0.5} + 0.8\, C\Big|_{t_g/t_{ge}=0.6}$$
$$C_{Rm}\Big|_{P_b/P_g=0.4} = 0.75\, C_{Rm}\Big|_{P_b/P_g=0.2} + 0.25\, C_{Rm}\Big|_{P_b/P_g=1}.$$

Polynomials are sensitive to coefficient precision, and the provided precision should be conserved when they are used in a model.

The normalized compliance is valid for $x_R/t_g < 0.8$, and the lumped model is not guaranteed to converge to a solution beyond this value.

The self radiation impedance is dependent on the frequency, the membrane radius, and also on the contact radius in collapsed mode. The mutual radiation impedance is dependent on the frequency, the membrane radius, the center-to-center distances between membranes and the contact radius in collapsed mode. Their values are introduced through lookup tables. There is a single lookup table for uncollapsed mode, while there are many lookup tables of collapsed mode for different $\overline{b}$ values. Impedance at intermediate $\overline{b}$ values should be interpolated. All of the lookup tables for "$R_1(ka) + j\,X_1(ka)$" are prepared as s2p files. The frequency parameter corresponds to ka in all files.

Table B.1: Parameter expressions in uncollapsed and collapsed modes

	Uncollapsed Mode		Collapsed Mode	
C_{Rm}	if $h_u(\overline{x}_R) < h_c(\overline{x}_R)$,	$= C_{Rm_0}\, h_u(\overline{x}_R)$ where $h_u(\overline{x}_R) = \begin{cases} \sum_{i=0}^{4} l_i \overline{x}_R^i & \text{if } (\sum_{i=0}^{4} l_i \overline{x}_R^i) > 1 \\ 1 & \text{otherwise} \end{cases}$	else	$= C_{Rm_0}\, h_c(\overline{x}_R)$ where $h_c(\overline{x}_R) = \begin{cases} \sum_{i=0}^{7} m_i \overline{x}_R^i & \text{if } (\sum_{i=0}^{7} m_i \overline{x}_R^i) > 0 \\ 0 & \text{otherwise} \end{cases}$
C	if $\overline{x}_R < X_C$,	$= C_0\, g(\sqrt{5}\,\overline{x}_R),\ g(u) = \frac{\tanh^{-1}(\sqrt{u})}{\sqrt{u}}$	else	$= C_0 \sum_{i=0}^{3} n_i \overline{x}_R^i$
f_R	if $\overline{x}_R < X_f$,	$= \frac{\sqrt{5}\,V^2\,C_0}{2t_{ge}} g'(\sqrt{5}\,\overline{x}_R),\ g'(u) = \frac{1}{2u}\left(\frac{1}{1-u} - g(u)\right)$	else	$= \frac{V^2\,C_0}{2\,t_{ge}} \sum_{i=1}^{3} i\, n_i\, \overline{x}_R^{i-1}$
b	if $\overline{x}_R < X_b$,	$= 0$	else	$= \mathrm{a} \sum_{i=0}^{6} p_i \overline{x}_R^i$
Z_{RR}	if $\overline{b} = 0$,	$Z(ka, \overline{b})$, with $\overline{b} = 0$	else	$Z(ka, \overline{b})$, with $\overline{b}$=0.05, 0.1, 0.15 ... 0.6

Table B.2: Table of Polynomial Coefficients for P_b/P_g=0.2 and t_g/t_{ge}=0.73

l_0	l_1	l_2	l_3	l_4			
43.324	-54.67	330.07	-876.04	877.55			
m_0	m_1	m_2	m_3	m_4	m_5	m_6	m_7
537.77	-7978.88	50668.32	-177920.22	372639.41	-465350.30	320838.34	-94225.80
X_C	X_F	n_0	n_1	n_2	n_3		
0.2579	0.3045	1.1297	-0.8666	6.0994	-0.1124		
X_b	p_0	p_1	p_2	p_3	p_4	p_5	p_6
0.32	13.0537	-145.5684	625.2401	-1305.847	1349.5205	-552.4294	0

Appendix C

Lumped Element Model in ADS

ADS[3] is a suitable circuit design environment for realizing the lumped element model of CMUT, as it is possible to introduce lookup tables and perform interpolation in multiple dimensions, define nonlinear parametrical equations both in time and frequency domains. The equivalent electrical circuit of a single CMUT cell modeled in ADS is given in Fig.C.1. SDD (Symbolically Defined Device) blocks are used for defining nonlinear voltage and current equations. The expressions for capacitance, capacitance derivative, and compliance are defined in "Variables and Equations" elements (not shown here). On the left side of the first

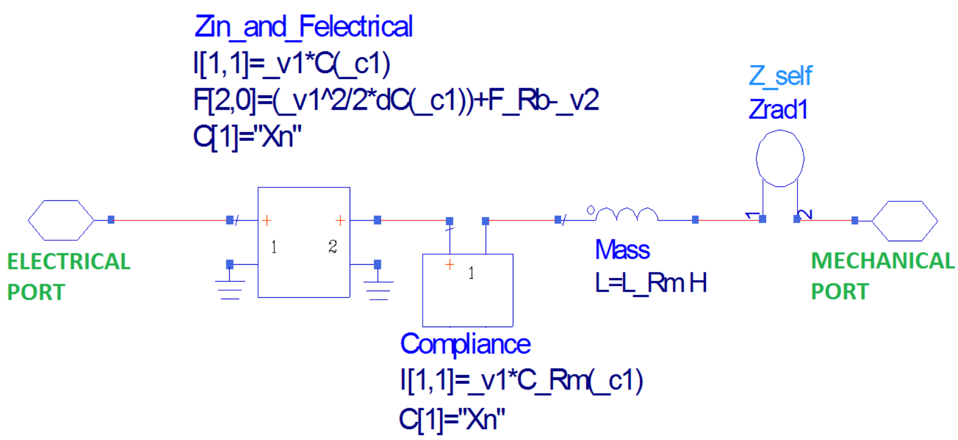

Figure C.1: The lumped element model of single CMUT cell in ADS.

[3] Advanced Design System from Agilent Technologies

SDD block, the electrical current is supplied to the electrical port; it is the time derivative of the instantaneous value of "$v_{IN}\,C$". The right side of the same block introduces the electrical force and the force due to ambient pressure, which is "$F_{Rb} + 0.5\,v_{IN}^2 \mathrm{d}C/\mathrm{d}x_R$". The second block defines the compliance. The current, which is velocity, is equal to the time derivative of the displacement (=restoring force x compliance). The inertial force of the membrane is represented with an inductor, inductance of which is equal to the membrane mass. And the last element included in the cell model is the self radiation impedance of the cell. In single CMUT simulations the mechanical port should be grounded as the cell model contains the self radiation impedance. In array simulations, it is used for introducing the mutual impedance between neighboring cells.

The self radiation impedance element is a component on its own, in which the impedance is defined through lookup tables as functions of contact radius and ka. In Fig.C.2 the self radiation impedance component is shown. Each of the "access_data" commands introduce the impedance as a function of ka at a fixed value of contact radius. This command reads the impedance from the lookup table in the related ".ds"" document, and interpolates in frequency domain. There are nine data readers for $\overline{b}$= 0, 0.5, 0.1, 0.15, 0.2, 0.3, 0.4, 0.5 and 0.6. In the SDD block, interpolation is performed between impedance functions of discrete $\overline{b}$. In order to interpolate instantaneously for changing contact radius in time domain, the rms velocity is separately convolved with each of the impedance functions of discrete $\overline{b}$ values, and interpolation is performed between the resulting force signals.

The mutual radiation impedance is used separately to connect the cells in an array as shown in Fig.C.4. In this figure, an 2x2 CMUT array model is given. Each CMUT is connected to other CMUTs through a mutual impedance component. As there are 6 pair connections between 4 CMUTs, we have 6 mutual impedance elements. For a closely packed array as seen on Fig.C.3, and the center-to-center distance between the CMUTs is $d1$ for all pairs, except the CMUT1-CMUT4 pair of distance $d2$. The mutual radiation impedance of each pair depends on their distance.

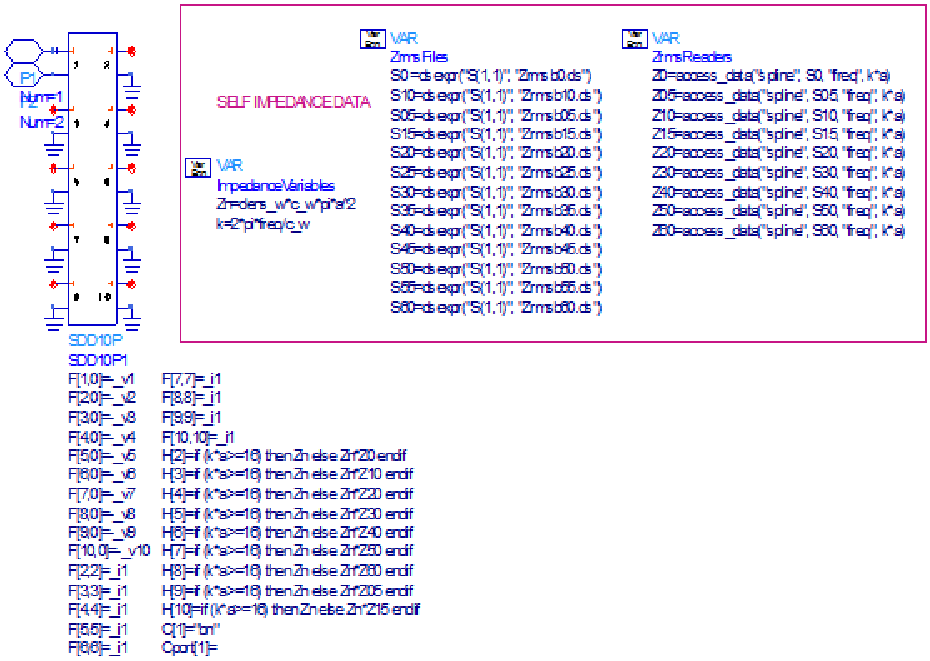

Figure C.2: The self radiation impedance model in ADS.

The mutual radiation impedance between two cells is defined with an SDD block. It calculates the force exerted on each of the cells due to their interaction. Similar to the self radiation impedance case, the mutual radiation impedance is introduced at discrete values of contact radius. In Fig.C.5, a mutual radiation impedance block is given. Small signal operation is assumed here, and the mutual impedance is introduced as function of the same $\bar{b}$ values for both cells. There are DACs (Data Access Components) (not shown here) for reading the impedance data from the document and interpolate in ka and kd domains. The impedance data produced by the DACs for each discrete value of $\bar{b}$ and d are used in the SDD. The velocity of a cell is convolved with the mutual radiation impedance at all discrete $\bar{b}$ values and interpolation is performed at instantaneous $\bar{b}$ to find the force exerted on the neighboring cell.

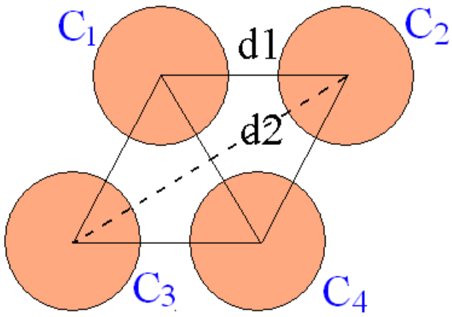

Figure C.3: Closely packed 2x2 CMUT array.

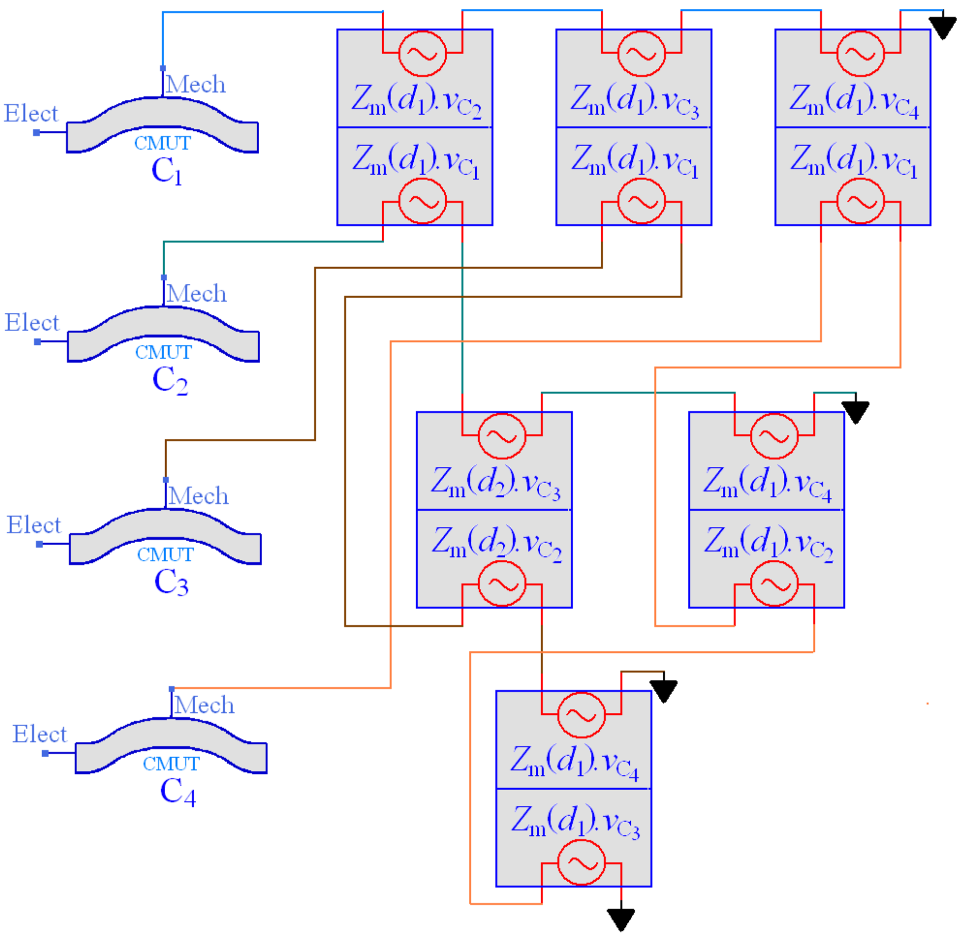

Figure C.4: The demonstration of mutual impedances in a 2x2 CMUT array.

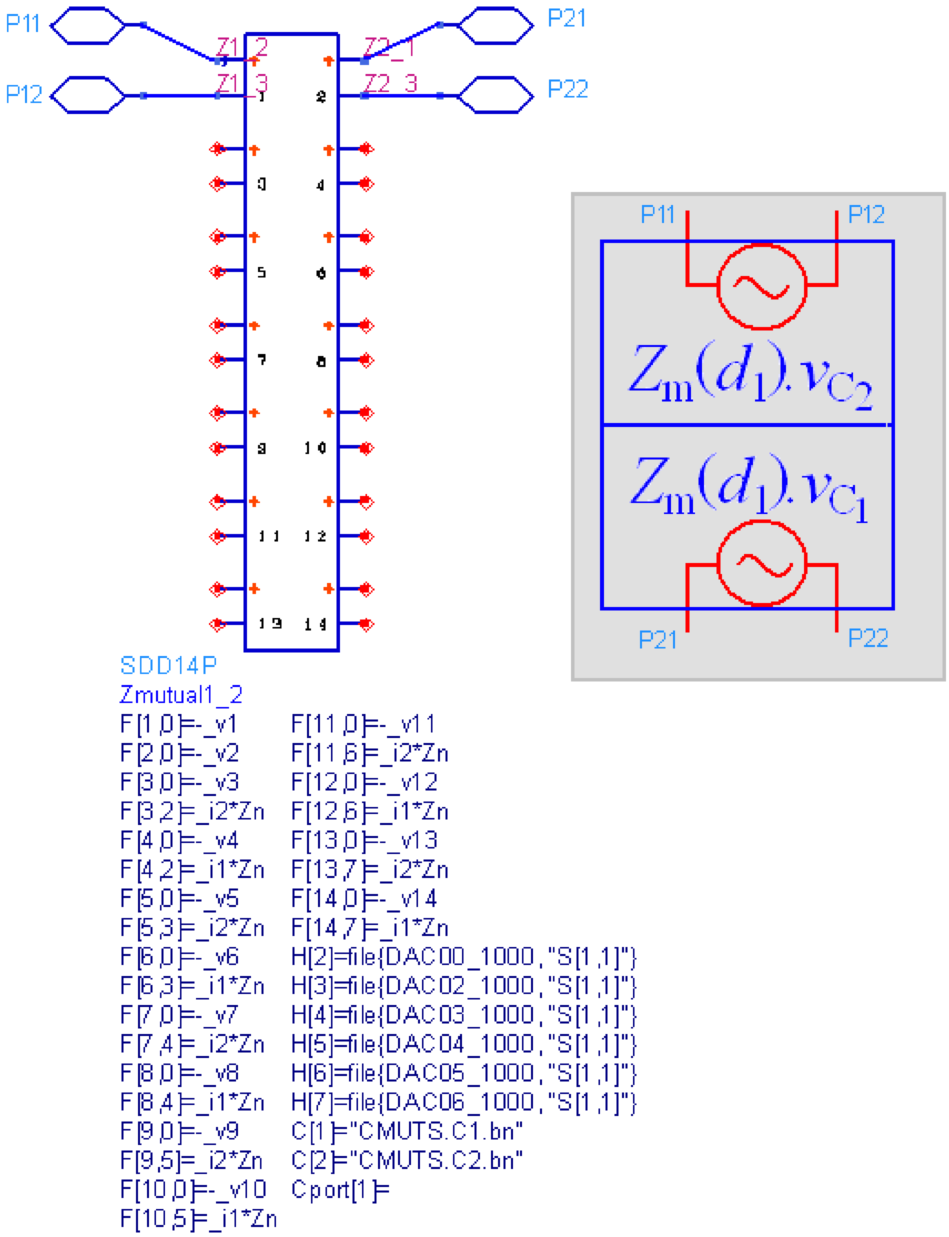

Figure C.5: The ADS model of mutual radiation impedance between 2 cells.

Bibliography

[1] V. Bavaro, G. Caliano, and M. Pappalardo, "Element shape design of 2-d CMUT arrays for reducing grating lobes," *IEEE Trans. Ultrason., Ferroelectr., Freq. Control*, vol. 55, pp. 308–318, 2008.

[2] A. Novell, M. Legros, N. Felix, and A. Bouakaz, "Exploitation of capacitive micromachined transducers for nonlinear ultrasound imaging," *IEEE Trans. Ultrason., Ferroelectr., Freq. Control*, vol. 56, pp. 2733–2743, 2009.

[3] T. G. Fisher, T. J. Hall, S. Panda, M. S. Richards, P. E. Barbone, J. F. Jiang, J. Resnick, and S. Barnes, "Volumetric elasticity imaging with a 2-D CMUT array," *Ultrasound in Medicine and Biology*, vol. 36, pp. 978–990, 2010.

[4] D. N. Stephens, M. ODonnell, K. Tomenius, A. Dentinger, D. Wildes, P. Chen, K. K. Shung, J. Cannata, B. T. Khuri-Yakub, O. Oralkan, A. Mahajan, K. Shivkumar, and D. J. Sahn, "Experimental studues with a 9 French forward-looking inter-cardiac imaging and ablation catheter," *J. Ultras. Med.*, vol. 28, pp. 207–215, 2009.

[5] F. L. Degertekin, R. O. Guldiken, and M. Karaman, "Annular-ring CMUT arrays for forward-looking ivus: transducer characterization and imaging," *IEEE Trans. Ultrason., Ferroelectr., Freq. Control*, vol. 53, pp. 474–482, 2006.

[6] G. Caliano, R. Carotenuto, E. Cianci, V. Foglietti, A. Caronti, A. Iula, and M. Pappalardo, "Design, fabrication and characterization of a capacitive micromachined ultrasonic probe for medical imaging," *IEEE Trans. Ultrason., Ferroelectr., Freq. Control*, vol. 52, pp. 2259–2269, 2005.

[7] A. Caronti, G. Caliano, R. Carotenuto, A. Savoia, M. Pappalardo, E. Cianci, and V. Foglietti, "Capacitive micromachined ultrasonic transducer (cmut)arrays for medical imaging," *Microelectronics Journal*, vol. 37, pp. 770–777, 2006.

[8] U. Demirci, A. S. Ergun, . Oralkan, M. Karaman, and B. T. Khuri-Yakub, "Forward-viewing CMUT arrays for medical imaging," *IEEE Trans. Ultrason., Ferroelectr., Freq. Control*, vol. 51, pp. 886–894, 2004.

[9] O. Oralkan, A. S. Ergun, C. H. Cheng, J. A. Jhonson, M. Karaman, T. H. Lee, and B. T. Khuri-Yakub, "Volumetric ultrasound imaging using 2-D CMUT arrays," *IEEE Trans. Ultrason., Ferroelectr., Freq. Control*, vol. 50, pp. 1581–1594, 2003.

[10] S. H. Wong, M. Kupnik, R. D. Watkins, K. Butts-Pauly, and B. T. Khuri-Yakub, "Capacitive micromachined ultrasonic transducers for therapeutic ultrasound applications," *IEEE Trans. Ultrason., Ferroelectr., Freq. Control*, vol. 57, pp. 114–123, 2010.

[11] S. T. Hansen, A. S. Ergun, W. Liou, B. A. Auld, and B. T. Khuri-Yakub, "Wide-band micromachined capacitive microphones with radio frequency detection," *J. Acoust. Soc. Am.*, vol. 116, pp. 828–842, 2004.

[12] I. O. Wygant, M. Kupnik, J. C. Windsor, W. M. Wright, M. S. Wochner, G. G. Yaralioglu, M. F. Hamilton, and B. T. Khuri-Yakub, "50 KHz capacitive micromachined ultrasonic transducers for generation of highly directional sound with parametric arrays," *IEEE Trans. Ultrason., Ferroelectr., Freq. Control*, vol. 56, pp. 193–203, 2009.

[13] M. I. Haller and B. T. Khuri-Yakub, "A surface micromachined electrostatic ultrasonic air transducer," *IEEE Trans. Ultrason., Ferroelectr., Freq. Control*, vol. 43, pp. 1–6, 1996.

[14] J. Zahorian, M. Hochman, T. Xu, S. Satir, G. Gurun, M. Karaman, and F. L. Degertekin, "Monolithic CMUT-on-CMOS integration for intravascular ultrasound applications," *IEEE Trans. Ultrason., Ferroelectr., Freq. Control*, vol. 58, pp. 2659–2667, 2011.

[15] I. O. Wygant, X. Zhuang, D. T. Yeh, . Oralkan, A. S. Ergun, M. Karaman, and B. T. Khuri-Yakub, "Integration of 2D CMUT arrays with front-end electronics for volumetric ultrasound imaging," *IEEE Trans. Ultrason., Ferroelectr., Freq. Control*, vol. 55, pp. 327–342, 2008.

[16] A. Nikoozadeh, I. O. Wygant, D. Lin, O. Oralkan, A. S. Ergun, D. N. Stephensen, K. E. Thomenius, A. M. D. D. Wildes, G. Akopyan, K. Shivkumar, A. Mahajan, D. J. Sahn, and B. T. Khuri-Yakub, "Forward-looking intercardiac ultrasound imaging using a 1-D CMUT array integrated with custom front-end electronics," *IEEE Trans. Ultrason., Ferroelectr., Freq. Control*, vol. 55, pp. 2651–2660, 2008.

[17] G. Gurun, P. Hassler, and F. L. Degertekin, "Front-end receiver electronics for high-frequency monolithic CMUT-on-CMOS imaging arrays," *IEEE Trans. Ultrason., Ferroelectr., Freq. Control*, vol. 58, pp. 1658–1668, 2011.

[18] I. Ladabaum, X. Jin, H. T. Soh, A. Atalar, and B. T. Khuri-Yakub, "Surface micromachined capacitive ultrasonic transducers," *IEEE Trans. Ultrason., Ferroelectr., Freq. Control*, vol. 45, pp. 678–690, 1998.

[19] B. Bayram, G. G. Yaralioglu, M. Kupnik, and B. T. Khuri-Yakub, "Acoustic crosstalk reduction method for CMUT arrays," in *Proceedings of the IEEE Ultrasonics Symposium*, pp. 590–593, 2006.

[20] G. G. Yaralioglu, A. S. Ergun, and B. T. Khuri-Yakub, "Finite-element analysis of capacitive micromachined ultrasonic transducers," *IEEE Trans. Ultrason., Ferroelectr., Freq. Control*, vol. 52, pp. 2185–2198, 2005.

[21] B. Bayram, G. G. Yaralioglu, M. Kupnik, A. S. Ergun, O. Oralkan, A. Nikoozadeh, and B. T. Khuri-Yakub, "Dynamic analysis of capacitive micromachined ultrasonic transducers," *IEEE Trans. Ultrason., Ferroelectr., Freq. Control*, vol. 52, pp. 2270–2275, 2005.

[22] A. Caronti, R. Carotenuto, G. Caliano, and M. Pappalardo, "The effects of membrane metallization in capacitive microfabricated ultrasonic transducers," *J. Acoust. Soc. Am.*, vol. 115, pp. 651–657, 2004.

[23] A. Caronti, A. Savoia, G. Caliano, and M. Pappalardo, "Acoustic coupling in capacitive microfabricated ultrasonic transducers: Modeling and experiments," *IEEE Trans. Ultrason., Ferroelectr., Freq. Control*, vol. 52, pp. 2220–2234, 2005.

[24] M. Buigas, F. M. Espinosa, G. Schmitz, I. Ameijeiras, P. Masegosa, and M. Dominguez, "Electro-acoustical characterization procedure for CMUTs," *Ultrasonics*, vol. 5, pp. 383–390, 2005.

[25] B. Bayram, M. Kupnik, G. G. Yaralioglu, O. Oralkan, D. Lin, X. Zhuang, A. S. Ergun, A. F. Sarioglu, S. H. Wong, and B. T. Khuri-Yakub, "Characterization of cross-coupling in capacitive micromachined ultrasonic transducers," in *Proceedings of the IEEE Ultrasonics Symposium*, pp. 601–604, 2005.

[26] O. Oralkan, B. Bayram, G. G. Yaralioglu, A. S. Ergun, M. Kupnik, D. T. Yeh, I. O. Wygant, and B. T. Khuri-Yakub, "Experimental characterization of collapse mode CMUT operation," *IEEE Trans. Ultrason., Ferroelectr., Freq. Control*, vol. 53, pp. 1513–1523, 2006.

[27] A. Nikoozadeh, B. Bayram, G. G. Yaralioglu, , and B. T. Khuri-Yakub, "Analytical calculation of collapse voltage of CMUT membrane," in *Proceedings of the IEEE Ultrasonics Symposium*, pp. 256–259, 2004.

[28] I. O. Wygant, M. Kupnik, and B. T. Khuri-Yakub, "Analytically calculating membrane displacement and the equivalent circuit model of a circular CMUT cell.," in *Proceedings of the IEEE Ultrasonics Symposium*, pp. 2111–2114, 2008.

[29] G. G. Yaralioglu, A. S. Ergun, B. Bayram, E. Haeggstrom, and B. T. Khuri-Yakub, "Calculation and measurement of electromechanical coupling coefficient of capacitive micromachined ultrasonic transducers," *IEEE Trans. Ultrason., Ferroelectr., Freq. Control*, vol. 50, pp. 449–456, 2003.

[30] A. Caronti, R. Carotenuto, and M. Pappalardo, "Electromechanical coupling factor of capacitive micromachined ultrasonic transducers," *J. Acoust. Soc. Am.*, vol. 113, pp. 279–288, 2003.

[31] W. P. Mason, *Electromechanical Transducers and Wave Filters.* Van Nostrand, New York, 1942.

[32] D. Certon, F. Teston, and F. Patat, "A finite difference model for CMUT devices," *IEEE Trans. Ultrason., Ferroelectr., Freq. Control*, vol. 52, pp. 2199–2210, 2005.

[33] A. Caronti, G. Caliano, A. Iula, and M. Pappalardo, "An accurate model for capacitive micromachined ultrasonic transducers," *IEEE Trans. Ultrason., Ferroelectr., Freq. Control*, vol. 49, pp. 159–167, 2002.

[34] G. Caliano, A. Caronti, M. Baruzzi, A. Rubini, A. Iula, R. Carotenuto, and M. Pappalardo, "Pspice modeling of capacitive microfabricated ultrasonic transducers," *Ultrasonics*, vol. 40, pp. 449–455, 2002.

[35] H. Koymen, A. Atalar, E. Aydogdu, C. Kocabas, H. K. Oguz, S. Olcum, A. Ozgurluk, and A. Unlugedik, "An improved lumped element nonlinear circuit model for a circular CMUT cell," *IEEE Trans. Ultrason., Ferroelectr., Freq. Control*, vol. 59, pp. 1791–1799, 2012.

[36] A. Lohfink and P. C. Eccardt, "Linear and nonlinear equivalent circuit modeling of CMUTs," *IEEE Trans. Ultrason., Ferroelectr., Freq. Control*, vol. 52, pp. 2163–2172, 2005.

[37] H. K. Oguz, S. Olcum, M. N. Senlik, V. Tas, A. Atalar, and H. Koymen, "Nonlinear modeling of an immersed transmitting capacitive micromachined ultrasonic transducer for harmonic balance analysis," *IEEE Trans. Ultrason., Ferroelectr., Freq. Control*, vol. 57, pp. 438–447, 2010.

[38] H. K. Oguz, A. Atalar, and H. Koymen, "Equivalent circuit-based analysis of CMUT cell dynamics in arrays," *IEEE Trans. Ultrason., Ferroelectr., Freq. Control*, vol. 60, pp. 1016–1023, 2013.

[39] X. Jin, O. Oralkan, F. L. Degertekin, and B. T. Khuri-Yakub, "Characterization of one-dimensional capacitive micromachined ultrasonic immersion transducer arrays," *IEEE Trans. Ultrason., Ferroelectr., Freq. Control*, vol. 48, pp. 750–759, 2001.

[40] S. Ballandras, M. Wilm, W. Daniau, A. Reinhardt, V. Laude, and R. Armati, "Periodic finite element/boundary element modeling of capacitive micromachined ultrasonic transducers," *J. Appl. Phys.*, vol. 97, p. 034901, 2005.

[41] M. N. Senlik, S. Olcum, H. Koymen, and A. Atalar, "Radiation impedance of an array of circular capacitive micromachined ultrasonic transducers," *IEEE Trans. Ultrason., Ferroelectr., Freq. Control*, vol. 57, pp. 969–976, 2010.

[42] S. Olcum, M. N. Senlik, and A. Atalar, "Optimization of the gain-bandwidth product of capacitive micromachined ultrasonic transducers," *IEEE Trans. Ultrason., Ferroelectr., Freq. Control*, vol. 54, pp. 2211–2219, 2005.

[43] H. Koymen, M. N. Senlik, A. Atalar, and S. Olcum, "Parametric linear modeling of circular CMUT membranes in vacuum," *IEEE Trans. Ultrason., Ferroelectr., Freq. Control*, vol. 54, pp. 1229–1239, 2007.

[44] B. Bayram, E. Haeggstrom, G. G. Yaralioglu, and B. T. Khuri-Yakub, "A new regime for operating capacitive micromachined ultrasonic transducers," *IEEE Trans. Ultrason., Ferroelectr., Freq. Control*, vol. 50, pp. 1184–1190, 2003.

[45] K. K. Park, O. Oralkan, and B. T. Khuri-Yakub, "A comparison between conventional and collapse-mode capacitive micromachined ultrasonic transducers in 10-mhz 1-d arrays," *IEEE Trans. Ultrason., Ferroelectr., Freq. Control*, vol. 60, pp. 1245–1255, 2013.

[46] Y. Huang, E. Haeggstrom, B. Bayram, X. Zhuang, A. S. Ergun, C. H. Cheng, and B. T. Khuri-Yakub, "Comparison of conventional and collapsed region operation of capacitive micromachined ultrasonic transducers," *IEEE Trans. Ultrason., Ferroelectr., Freq. Control*, vol. 53, pp. 1918–1932, 2006.

[47] B. Bayram, . Oralkan, A. S. Ergun, E. Hggstrm, G. G. Yaralioglu, and B. T. Khuri-Yakub, "Capacitive micromachined ultrasonic transducer design for high power transmission," *IEEE Trans. Ultrason., Ferroelectr., Freq. Control*, vol. 52, pp. 326–339, 2005.

[48] S. Olcum, Y. Yamaner, A. Bozkurt, H. Koymen, and A. Atalar, "Deep collapse operation of capacitive micromachined ultrasonic transducers," *IEEE Trans. Ultrason., Ferroelectr., Freq. Control*, vol. 58, pp. 2475–2483, 2011.

[49] S. Olcum, Y. Yamaner, A. Bozkurt, H. Koymen, and A. Atalar, "An equivalent circuit model for transmitting capacitive micromachined ultrasonic transducers in collapse mode," *IEEE Trans. Ultrason., Ferroelectr., Freq. Control*, vol. 58, pp. 1468–1476, 2011.

[50] S. Timoshenko and S. W. Woinowsky-Krieger, *Theory of Plates And Shells*. NY: McGraw Hill, 1959.

[51] A. Ozgurluk, A. Atalar, H. Koymen, and S. Olcum, "Radiation impedance of collapsed capacitive micromachined ultrasonic transducers," *IEEE Trans. Ultrason., Ferroelectr., Freq. Control*, vol. 59, pp. 1301–1308, 2012.